Investigation of neural and biomechanical impairments leading to pathological toe and heel gaits using neuromusculoskeletal modelling

Alice Bruel[1] �’, Salim Ben Ghorbel[1], Andrea Di Russo[1], Dimitar Stanev[1], Stéphane Armand[2], Grégoire Courtine[3] and Auke Ijspeert[1]
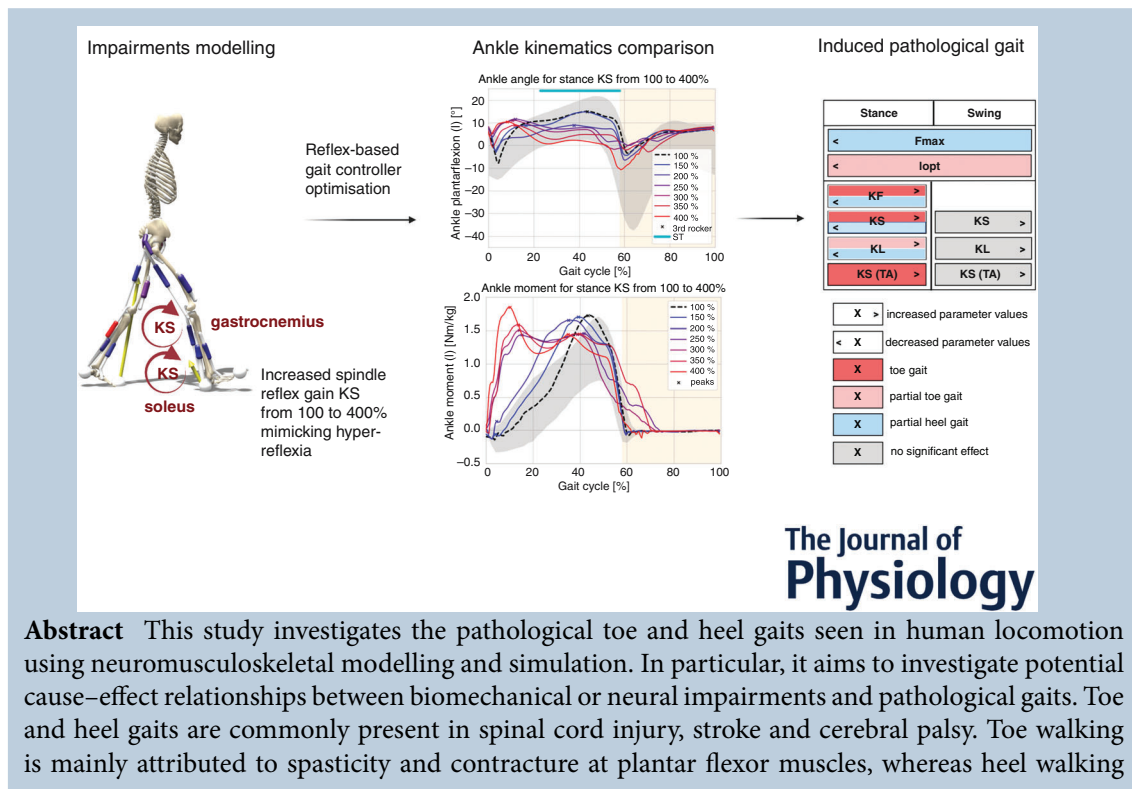
[1]*BioRobotics Laboratory, EPFL, Lausanne, Switzerland*
[2]*Kinesiology Laboratory – HUG/UNIGE, Switzerland*
[3]*Upcourtine EPFL, USA*

Edited by: Richard Carson & Vaughan Macefield

The peer review history is available in the Supporting information section of this article (https://doi.org/10.1113/JP282609#support-information-section).

Abstract This study investigates the pathological toe and heel gaits seen in human locomotion using neuromusculoskeletal modelling and simulation. In particular, it aims to investigate potential cause–effect relationships between biomechanical or neural impairments and pathological gaits. Toe and heel gaits are commonly present in spinal cord injury, stroke and cerebral palsy. Toe walking is mainly attributed to spasticity and contracture at plantar flexor muscles, whereas heel walking

Alice Bruel graduated from the French Engineering School Ecole Polytechnique and received an MSc in Life of Science with a Minor in Neuroprosthetics at the Swiss Institute of Technology in Lausanne (EPFL). During her Master's degree, she completed a project at the BIOROB laboratory related to the modelling of pathological gaits. She has since joined BIOROB and NeuroRestore in 2020 as a PhD student co-supervised by Professors Ijspeert and Courtine. She is involved in a project funded by the Human Brain Project (HBP) where she is studying the roles of spinal circuits in human motor control through neuromusculoskeletal modelling.

can be attributed to muscle weakness of biomechanical or neural origin. To investigate the effect of these impairments on gait, this study focuses on the soleus and gastrocnemius muscles as they contribute to ankle plantarflexion. We built a reflex circuit model based on previous work by Geyer and Herr with additional pathways affecting the plantar flexor muscles. The SCONE software, which provides optimisation tools for 2D neuromechanical simulation of human locomotion, is used to optimise the corresponding reflex parameters and simulate healthy gait. We then modelled various bilateral plantar flexor biomechanical and neural impairments, and individually introduced them in the healthy model. We characterised the resulting simulated gaits as pathological or not by comparing ankle kinematics and ankle moment with the healthy optimised gait based on metrics used in clinical studies. Our simulations suggest that toe walking can be generated by hyperreflexia, whereas muscle and neural weaknesses partially induce heel gait. Thus, this 'what if' approach is deemed of great interest as it allows investigation of the effect of various impairments on gait and suggests an important contribution of active reflex mechanisms to pathological toe gait.

Corresponding author Alice Bruel: BioRobotics Laboratory, EPFL, 1015 Lausanne, Switzerland.   Email: alice.bruel@epfl.ch

Abstract figure legend Various biomechanical and neural impairments are individually modelled at the level of the plantar flexor muscles in a musculoskeletal model and a complex reflex circuit-based gait controller. For instance, as shown on the left, the plantar flexor spindle reflex gain (KS) is increased to mimic hyperreflexia. The gait controller is then optimised for each of the impaired conditions and the resulting gaits are characterised as pathological based on ankle kinematics and ankle moment metrics used in clinical studies. Thus, this 'what if' approach allows the investigation of the effect of various impairments on gait presented in the table on the right.

Key points

- Pathological toe and heel gaits are commonly present in various conditions such as spinal cord injury, stroke and cerebral palsy.
- These conditions present various neural and biomechanical impairments, but the cause–effect relationships between these impairments and pathological gaits are difficult to establish clinically.
- Based on neuromechanical simulation, this study focuses on the plantar flexor muscles and builds a new reflex circuit controller to model and evaluate the potential effect of both neural and biomechanical impairments on gait.
- Our results suggest an important contribution of active reflex mechanisms to pathological toe gait.
- This 'what if' based on neuromechanical modelling is thus deemed of great interest to target potential causes of pathological gait.

Introduction

Human locomotion relies on complex interactions between the musculoskeletal system, spinal circuits, sensory reflex pathways, descending pathways and the environment (Rossignol et al., 2006). Neuro-musculoskeletal modelling is a powerful tool to study these complex interactions and the contribution of each of these motor control components, as it allows for the systematic evaluation of different models and parameters. Neuromusculoskeletal modelling has thus been used to study and understand human locomotion. Nevertheless, abnormal gaits resulting from illness or injury are less often modelled. Indeed, pathological gaits can have several causes ranging from biomechanical to neural

impairments. Neuromusculoskeletal modelling can help target and understand impaired mechanisms leading to pathological gaits by evaluating a model with altered parameters (Ong et al., 2019).

This study aims to investigate the effect of both biomechanical and neural impairments on gait using neuromusculoskeletal simulation. Two pathological gaits common in several conditions such as spinal cord injury (SCI), stroke and cerebral palsy (CP) are studied, namely toe and heel gaits. Toe walking, also called equinus gait, is a gait in which there is continuous ankle plantarflexion throughout the stance phase (Nieuwenhuys et al., 2015). This gait deviation is mainly attributed to spasticity and contracture at plantar flexor muscles that are present in

SCI, stroke and CP conditions (Armand et al., 2016; Attias et al., 2017; Crenna, 1998; Lamontagne et al., 2002; Matjacic et al., 2006; Van Der Salm et al., 2005). The most common definition of spasticity is from Lance et al. (1980) stating that spasticity is 'a motor disorder, characterised by a velocity-dependent increase in tonic stretch reflexes, resulting from hyperexcitability of the stretch reflex'. Spastic hyperreflexia is mainly due to increased alpha motor neuron excitability (Leech et al., 2018; Marque et al., 2001), reduction of presynaptic inhibition (Calancie et al., 1993; Faist et al., 1994) and reduction of reciprocal inhibition (Knikou & Mummidisetty, 2011) to reciprocal facilitation (Crone et al., 2003; Xia & Rymer, 2005). Biomechanical changes within both muscle–tendon unit cells and extracellular matrix collagen fibres can also contribute to spastic conditions by inducing a stiffer muscle–tendon unit (Diong et al., 2012; Lieber et al., 2004). In the long term, spasticity can also lead to the shortening of the muscle–tendon complex resulting in muscle contracture. For its part, heel walking, also called calcaneus gait, is a gait in which there is an excessive ankle dorsiflexion during the stance phase (Nieuwenhuys et al., 2015). This gait deviation is mainly attributed to muscle weakness that is also present in SCI, stroke and CP conditions (Armand et al., 2016; Bohannon, 2007; Elder et al., 2003; Thomas et al., 1997). Muscle weakness is a lack of muscle strength that can be induced by muscle diseases, but also by deficits in the neural drive leading to muscle atrophy (Thomas et al., 1997). Thus, both toe and heel gaits present impaired mechanisms that can have neural or biomechanical origins.

Several neuromechanical models of human locomotion have been developed over the years. The existence and contribution of central pattern generators (CPGs) producing rhythmic patterns in spinal circuits appear to be fundamental for lower vertebrate locomotion (Kiehn, 2016). However, they are still discussed for human locomotion that would rely on more important sensory reflex pathways and descending pathways (Minassian et al., 2017; Sinkjær et al., 2000). Several neuromechanical models include both CPGs and sensory feedbacks to simulate human locomotion (Aoi et al., 2019; Kuo & Ryu, 2021; Taga, 1995). On another note, Geyer and Herr (2010) developed a purely reflex-based model encoding the principles of legged mechanics and reproducing human walking kinematics, dynamics and muscle activation. Song and Geyer (2015) extended this model with additional muscle velocity feedbacks in particular, and were able to generate various behaviours of human locomotion from walking on a slope to running. Ong et al. (2019) also simulated human walking through a model based on muscle length, velocity and force reflexes. The modulation of walking speed, step length and step duration by these reflexes was further studied by Di Russo et al. (2021). These models including more reflex pathways

are more in line with physiological mechanisms. The present study similarly builds on Geyer and Herr's model by introducing additional reflex pathways affecting the soleus (SOL) and gastrocnemius (GAS), and their antagonist muscle tibialis anterior (TA) to more closely reproduce physiological mechanisms and simulate impairments. This study focuses in particular on the SOL and GAS muscles as they contribute to ankle plantarflexion, and are thus usually involved in both toe and heel gaits.

Previous studies also modelled spasticity or muscle weakness through neural or biomechanical impairments. Van der Krogt et al. (2016) modelled spasticity in CP children with velocity-dependent stretch reflex. That model replicated hamstring (HAMS) EMG global shape during passive stretching, but did not reproduce EMG fast variations. Falisse et al. (2018) also studied spasticity in CP children and compared three models based on velocity, acceleration and force feedback. The force-related model predicted HAMS and GAS activity that better correlated with measured activity during gait compared with the two other models. Jansen et al. (2014) simulated increased length and velocity feedbacks and altered reflex modulation patterns of lower limb muscles. They reproduced hemiparetic gait deviations, but they could not distinguish the contributions of the two pathways. Song and Geyer (2018) simulated the major contribution of loss of muscle strength and contraction speed in walking speed and efficiency decline with ageing based on Song and Geyer (2015). Waterval et al. (2021) also reproduced most gait changes due to bilateral plantar flexor weakness based on Geyer and Herr's model. Similarly, Ong et al. (2019) modelled SOL and GAS weakness and contracture with respectively reduced maximal isometric force and reduced muscle fibre optimal length. Severe plantar flexor weakness resulted in heel walking, whereas severe contracture resulted in toe walking simulation.

By investigating the effect of both biomechanical and neural impairments on gait, the present study addresses the following question: can we identify specific biomechanical and neural causes inducing the pathological toe and heel gaits?

For answer this, we developed a reflex circuit model by extending Geyer and Herr's reflex circuits with additional pathways affecting the SOL and GAS muscles, and their antagonist muscle TA. The model introduces additional force, spindle and length direct pathways for these three muscles and reciprocal spindle pathways between plantar flexors and TA. The SCONE software (Geijtenbeek, 2019), which provides optimisation tools for 2D neuromechanical simulation of human locomotion based on Geyer and Herr's work, is used to optimise the parameters of this reflex circuit model and simulate a healthy gait. We then modelled various bilateral plantar

flexor biomechanical and neural impairments through decreased or increased parameter values. Biomechanical parameters are altered to model muscle weakness and reduced muscle fibre length. Regarding reflex parameters, they are modified to model hyperreflexia, reduction of presynaptic inhibition, reduction of reciprocal inhibition and neural weakness. We individually introduced each of these modelled impairments in the healthy model and simulated the gait resulting from new optimisation. All these simulated gaits then need to be characterised as pathological or not. To do so, we compared ankle kinematics and ankle moment of each impaired evaluation with the healthy optimisation based on metrics used in clinical studies.

Methods

This section presents the methods, including the SCONE software simulation framework, the developed reflex circuit model, the modelled biomechanical and neural impairments and the pathological gait characterisation. All the necessary files to reproduce this study are provided in a GitHub repository shared in the Additional information section.

SCONE simulation

Gait simulations were performed with the SCONE software (Geijtenbeek, 2019) that is based on the following four blocks:

- An OpenSim musculoskeletal model: here we use a model based on Delp et al. (1990). This model represents an adult of about 1.8 m and 75 kg. It is constrained in the sagittal plane with three degrees

of freedom (DOF) per leg, namely at the hip, knee and ankle joints, and a 3 DOF planar joint between the pelvis and the ground. This model is composed of seven Hill-based muscles with tendon compliance (Millard et al., 2013) per leg shown in Fig. 1: gluteus maximus (GMAX), HAMS, iliopsoas (ILSPO), vasti (VAS), GAS, SOL and TA. Muscle–tendon parameters are taken from Delp et al. (1990), which is based on experimental data. To estimate the ground reaction forces, a compliant contact model is used with one viscoelastic Hunt–Crossley sphere representing the heel and another one representing the toes (Hunt & Crossley, 1975).

- A controller: here we use a reflex circuit controller adapted from Geyer & Herr's (2010) model. This controller is composed of several state-dependent control law primitives, including feedforward, muscle reflex and pelvis tilt proportional-derivative primitives. These different components are detailed below with the extended reflex circuit model that is developed for this study.

- Measures that are minimised through the optimisation as components of the cost function: here we considered the following human walking goals as measures:

  – A gait measure penalising falling and walking speed lower than a minimum speed:

This gait measure takes values between 1, when the model falls at the first step, and 0, when the model does not fall and the velocity condition is met. The model is considered to fall when the ratio between its centre of mass height (h_{COM}) to the initial state ($h_{COM,i}$) is smaller than a termination height threshold set to 0.8 ($\frac{h_{COM}}{h_{COM,i}} <$ 0.8). For each step (s), the step end time ($t_{s,end}$) and the step speed (v_s) are then respectively compared to
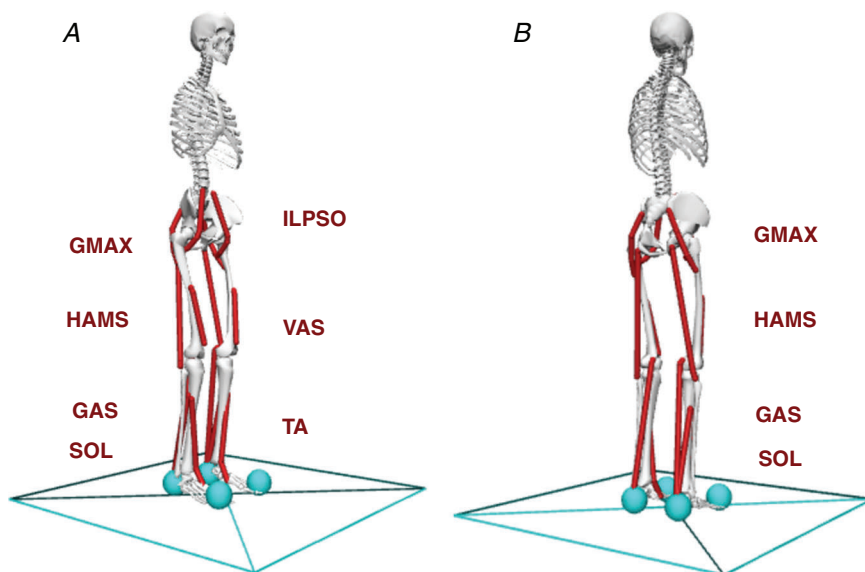

Figure 1. OpenSim musculoskeletal model composed of three degrees of freedom per leg, at the hip, knee and ankle joints, and seven Hill-based muscles per leg
A, front view with iliopsoas (ILPSO), vasti (VAS) and tibialis anterior (TA). *B*, back view with gluteus maximus (GMAX), hamstrings (HAMS), gastrocnemius (GAS) and soleus (SOL). [Colour figure can be viewed at wileyonlinelibrary.com]

potential falling time (t_{fall}) and a minimum speed (v_{min}) set to 1.0 m/s. The resulting gait measure is:

$$J_{gt} = 1 - \frac{1}{N_{Steps}} \sum_{s \in Steps} p\left(t_{s,end}, v_s\right) \quad (1)$$

where $\begin{cases} p(t_{s,end}, v_s) = 0, \ if \ t_{s,end} = t_{fall} \\ p(t_{s,end}, v_s) = \frac{v_s}{v_{min}}, \ if \ v_s < v_{min}. \\ p(t_{s,end}, v_s) = 1, \ if \ v_s \geq v_{min} \end{cases}$

– An effort measure from Wang et al. (2012) minimising muscle metabolic energy:

$$J_{eff} = \frac{1}{m * L}\left(\dot{B} + \sum_{m \in Muscles} \dot{E}_m\right) \quad (2)$$

where m is the body mass, L is the travelled distance, $\dot{B}$ is the basal metabolic energy rate set to 1.51 times the body mass and $\dot{E}_m$ is the mean rate of metabolic energy expenditure for a given muscle throughout the simulation.

– A joint measure penalising non-physiological movements by minimising the knee limit force (F_{lim}) representing knee ligaments (Veerkamp et al., 2021). This measure also penalises the overextension of the other joints (ankle, hip, pelvis) by penalising the corresponding joint angles (α_{jt}) overcoming experimental ranges from Schwartz et al. (2008) ($[\alpha_{jt,min}, \alpha_{jt,max}]$). These experimental ranges are more precisely [0, 15]° for the pelvis retroversion–anteversion, [−20, 40]° for the hip extension–flexion and [−30, 15]° for the plantarflexion–dorsiflexion. The resulting joint measure is:

$$J_{jt} = \int_0^{t_{end}} F_{lim}\ (t)\ dt + \sum_{jt \in Joints} \int_0^{t_{end}}$$

$$\times max\left(\alpha_{jt}\ (t) - \alpha_{jt,max}, \alpha_{jt,min} - \alpha_{jt}\ (t)\ , 0\right) dt \quad (3)$$

These measures finally result in the following cost of function with the same weights as Ong et al. (2019) who defined them to balance competing objectives:

$$J_{tot} = w_{gt}\ * J_{gt} + w_{eff} * J_{eff} + \sum_{jt \in Joints} w_{jt} * J_{jt} \quad (4)$$

with $w_{gt} = 100$, $w_{eff} = 0.1$ *and* $w_{jt} = 1$

- An optimiser that optimises the initial conditions and controller parameters to minimise the previous measures: here the Covariance Matrix Adaptation Evolutionary Strategy (CMA-ES) from Igel et al. (2007) is applied to optimise about 100 parameters of the reflex circuit model. The population size of each generation ($\bar{\lambda}$) is set to 40 and the initial step size (σ) is set to 5.

This optimisation scheme is thus used to generate a healthy gait of 15 s. We stopped the optimisation when a mean diminution of the cost function <5% was reached between successive optimisation steps. About 5000 generations of CMA-ES were necessary to fulfil this condition. The corresponding simulated gait is stable and reproduces human walking kinematics and muscle activation as presented in more details below. The generation of pathological optimisations is described below.

Reflex circuit model

This subsection first presents the baseline reflex-based model developed by Geyer & Herr (2010). Our extension, which introduces additional pathways affecting the SOL and GAS muscles, and their antagonist muscle TA, is then presented.

Baseline reflex circuit model from Geyer and Herr. The baseline reflex circuit model is taken from Geyer and Herr's work with a reflex-based controller composed of several state-dependent control law primitives, including feedforward, muscle reflex and pelvis tilt proportional–derivative primitives as summarised in Fig. 2. A feedforward component provides a feedforward constant excitation to each muscle actuator modelling supraspinal drive. A muscle reflex primitive accepts as input the sensed normalised fibre length (L) or force (F).

	Stance			Swing	
	ES	MS	PS	S	LP
GMAX	PD+, C		C	F+	
HAMS	PD+, C			F+	
ILPSO	PD-, C		C	L+, L- (HAMS)	
VAS	C, F+				
SOL	F+				
GAS	F+				
TA	L+, F- (SOL)				

Figure 2. Reflex-based controller from Geyer and Herr
The controller is composed of feedforward (*C*), muscle reflex and pelvis tilt proportional-derivative (PD) primitives. Muscles are indicated by acronyms on the left. The reflex primitives are based on normalised muscle length (*L*) or force (*F*). They are positive feedback laws onto the same muscle (*L*+, *F*+), except the negative force feedback law from the SOL to the TA (*F*−$_{SOL}$) and length feedback law from the HAMS to the ILPSO (*L*−$_{HAMS}$). All these components are state-dependent with five states: early stance (ES), mid-stance (MS), pre-swing (PS), swing (S) and landing preparation (LP).

A muscle reflex primitive based on X then provides the following muscle excitation:

$$u_X = KX * [X(t - t_D) - X_0]_+ \qquad (5)$$

where KX is the reflex gain, the sign of which is indicated by the sign of the reflex (X+) or (X−), t_D is the reflex delay, X_0 is the reflex offset and $[x]_+ = max(x, 0)$.

Geyer and Herr's reflex primitives are positive feedback laws onto the same muscle, except the negative force feedback law from the SOL to the TA and length feedback law from the HAMS to the ILPSO. Reflex gains and offsets are optimised parameters, whereas reflex delays are fixed. Similarly, the pelvis tilt proportional derivative component provides such muscle excitation based on the pelvis angle and angular velocity for balance control. Muscle activation is then calculated from the sum of the muscle excitation using a first-order dynamic model, with activation and deactivation time constants of 10 and 40 ms, respectively.

Moreover, all these primitives are state-dependent on five states: early stance (ES), mid-stance (MS) and pre-swing (PS) for the stance phase, and swing (S) and landing preparation (LP) for the swing phase. This state dependency reproduces the phase-dependent modulation of neural pathways that occurs during gait. Neural feedbacks are indeed modulated between stance and swing phases due to presynaptic inhibition and other descending modulation mechanisms (Boschges & El Manira, 1998; Meunier & Pierrot-Deseilligny, 1998; Prochazka, 1989). Thresholds for the ground reaction force (GRF) on the ipsilateral foot and for the distance between the ipsilateral foot and pelvis are optimised to determine the transition between these states.

Ton order to better link Geyer and Herr's reflex rules to actual neural circuits and to facilitate the introduction of additional reflexes (see next section), we have mapped the rules to a neural circuit for SOL, GAS and TA muscles in Fig. 3A. The Ib afferent disynaptic pathway from plantar flexor golgi tendon organ (GTO) to alpha motor neuron provides the force feedback. The corresponding reflex is defined as positive and represented through an excitatory interneuron during the stance states to model Ib facilitation during late stance (Af Klint et al., 2010; Faist et al., 2006). Such a pathway providing feedback from a muscle to itself is referred to as a direct pathway. By opposition, a pathway that provides feedback from a muscle to its antagonist's muscle is a reciprocal pathway. TA is also included in this representation as it is coupled with SOL by such an Ib reciprocal pathway. This force reflex from the SOL to the TA is defined as negative and represented through an inhibitory interneuron to model reciprocal inhibition. TA also receives positive length feedback from its muscle spindle through a II afferent disynaptic pathway. Regarding pathway delays, Ong et al. (2019) fixes direct reflex delays to 20 ms (compared with

5 and 10 ms for hip and knee muscles, respectively). In contrast, Ong et al. (2019) fixes Ib reciprocal reflex from the SOL to the TA delay to 40 ms as reciprocal reflexes involve longer pathways and are thus more delayed (Crone et al., 1987). Nevertheless, note that these delays are shorter than those recorded experimentally by an order of 50% (Frijns et al., 1997).

More complex reflex circuit model for the SOL, GAS and TA muscles. Based on the previous model, we developed a more complex reflex circuit model with additional SOL, GAS and TA pathways. Spindle Ia and II afferent direct pathways are added to study three types of feedback, namely force, spindle and length direct feedbacks. The Ia afferent pathway indeed provides major muscle velocity and length feedback and is involved in the common stretch reflex. As plantar flexors Ib and TA II direct pathways in Ong et al. (2019), we set the delay of these direct pathways to 20 ms. Moreover, reciprocal inhibition pathways between the antagonist's muscles are also present and important in physiological mechanisms. Indeed, if the antagonist's muscles contract simultaneously, they work against each other, leading to extra effort and potential muscle tear. Reciprocal inhibition pathways prevent such co-contraction and, in this way, participate in movement facilitation and muscle protection. Thus, to study these determinant pathways, we also introduced spindle Ia reciprocal reflexes between plantar flexors and TA in the model as represented in Fig. 3B and D. For the SOL to TA Ib reciprocal pathway, we modelled these reciprocal reflexes with disynaptic pathways and we set their delays to 40 ms. To summarise, the additional pathways introduced in this more complex model are tabulated in Fig. 4 and are as follows:

- SOL, GAS and TA Ia direct pathway: this pathway provides velocity and length feedback from the muscle spindle. The corresponding primitive in the SCONE controller is based on the spindle rate from Prochazka (1999) as a function of both muscle stretch velocity and length $(\alpha * v^{0.6} + \beta * l + \gamma)$. It is modelled with a monosynaptic pathway and is defined as positive to reproduce the excitatory stretch reflex (Pierrot-Deseilligny & Burke, 2012). This reflex is mainly involved in plantar flexor activation during gait (Yang et al., 1991).
- SOL and GAS II direct pathway: this pathway provides length feedback from the muscle spindle. It is modelled with a disynaptic pathway and is defined as positive to mimic the disynaptic II excitation in line with the literature (Lundberg et al., 1987; Pierrot-Deseilligny & Burke, 2012).
- SOL and GAS Ib direct pathway during the swing: as described above, this pathway provides force feedback from the GTO. It is modelled with a disynaptic

pathway in line with the literature (Pierrot-Deseilligny & Burke, 2012; Stephens & Yang, 1996). It is defined as positive during the stance states to reproduce the plantar flexor Ib facilitation that occurs during late stance (Af Klint et al., 2010; Faist et al., 2006). In contrast, it is defined as negative during the swing states to reproduce the common Golgi tendon reflex regulating muscle tension.

- Plantar flexor to TA Ia reciprocal pathway: this pathway provides negative spindle feedback from the plantar flexors to the TA. It is modelled with a disynaptic inhibitory pathway and is defined as negative to mimic the common reciprocal inhibition between antagonist muscles (Pierrot-Deseilligny & Burke, 2012).
- TA to plantar flexor Ia reciprocal pathway: this pathway similarly provides negative spindle feedback from

the TA to the plantar flexors through a disynaptic inhibitory pathway to mimic reciprocal inhibition.

As detailed above, we fixed the signs of the controller primitives (as opposed to being open for optimisation) as there is experimental evidence of the excitatory or inhibitory nature of the corresponding pathways that we wanted to account for (Pierrot-Deseilligny & Burke, 2012).

Modelled impairments

The effect of biomechanical and neural impairments is investigated by individually modifying various bilateral plantar flexor biomechanical and reflex parameters. Biomechanical parameters are altered to reproduce plantar flexor weakness and reduced muscle fibre length.
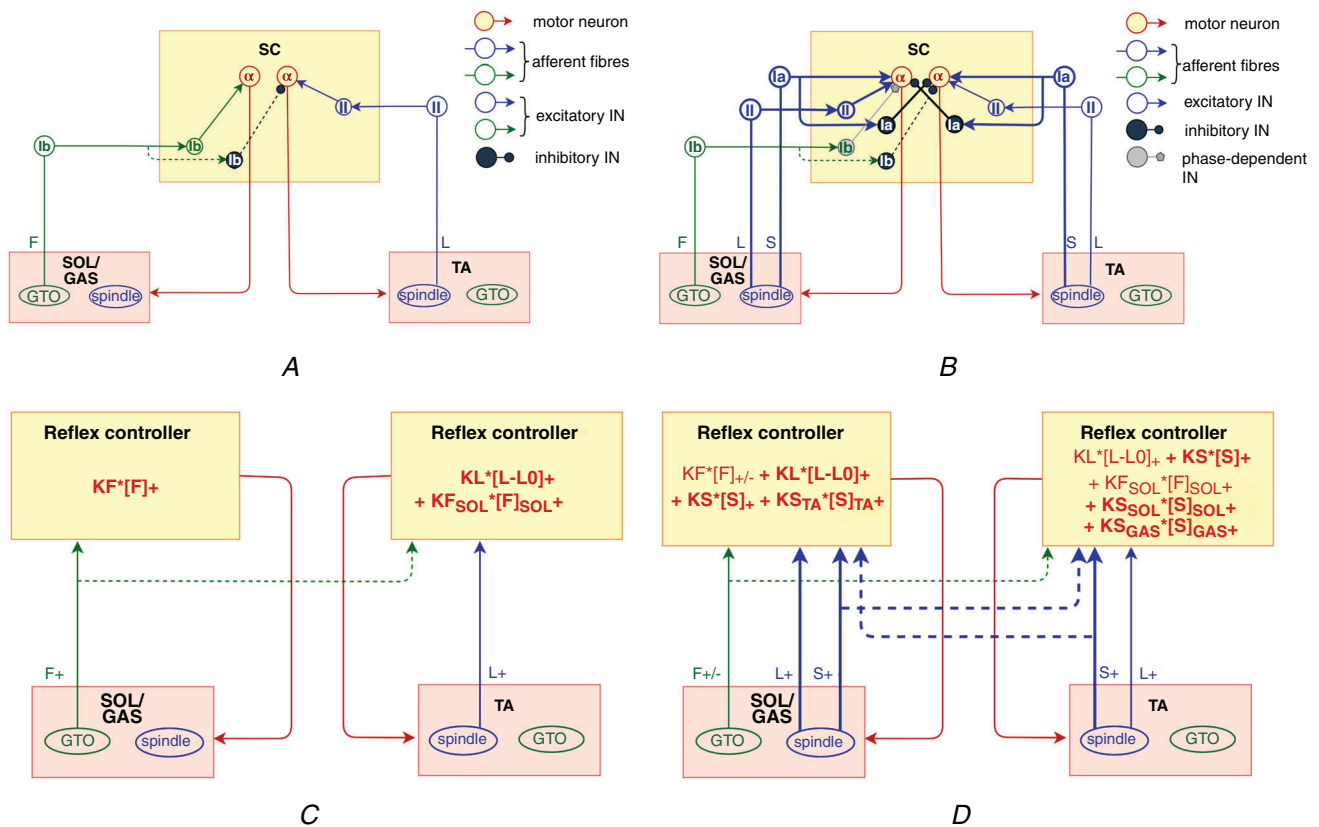

Figure 3. Representations of SOL, GAS and TA reflex circuit model from Geyer and Herr (left) and our extended model including additional direct and reciprocal pathways (right)
A, neural circuit implementation of Geyer and Herr's reflex rules for SOL, GAS and TA muscles. The Ib disynaptic pathway from plantar flexor GTO to alpha motor neuron provides positive force (F) feedback, Ib reciprocal pathway from SOL GTO to TA alpha motor neuron provides negative force feedback and II disynaptic pathway from TA spindle to plantar flexor alpha motor neuron provides positive length (L) feedback. B, neural circuit implementation of our extended model: the additional pathways are indicated in bold. The Ia monosynaptic pathway from muscle spindle to alpha motor neuron provides positive spindle (S) feedback reproducing the stretch reflex. The II disynaptic pathway from muscle spindle to alpha motor neuron provides positive length feedback. The Ia reciprocal pathway from muscle spindle to antagonist alpha motor neuron provides negative spindle feedback mimicking reciprocal inhibition. C, controller reflex primitives corresponding to A. D, controller reflex primitives corresponding to B: SOL, GAS and TA direct and reciprocal L and S reflexes are added to the previous primitives. [Colour figure can be viewed at wileyonlinelibrary.com]

As for reflex parameters, they are modified to mimic plantar flexor hyperreflexia, reduction of presynaptic and reciprocal inhibition, and neural weakness. This subsection presents these parameters of interest. For each of them, SOL and GAS values are altered simultaneously and by the same percentage of the corresponding healthy optimisation values as these muscles are agonists and commonly impaired simultaneously (Armand et al., 2016; Neyroud et al., 2017; Van der Krogt et al., 2010).

Biomechanical impairments. Muscle biomechanical properties are defined in the OpenSim musculoskeletal model through maximal isometric force, optimal muscle fibre length, tendon slack length, pennation angle parameters, and muscle fibre and tendon force–length and force–velocity curves. We investigate the following parameters:

- Plantar flexor maximal isometric force, F_{max}: this parameter is evaluated with decreased values to model muscle weakness.
- Plantar flexor fibre optimal length, l_0^{fib}: this parameter is evaluated with decreased values to reproduce muscle contracture.

Neural impairments. Impairments of both direct and reciprocal pathways affecting the plantar flexors are modelled. As mentioned above, reflex feedbacks are modulated between gait phases. Thus, we investigate each of the following reflexes during the stance or swing states:

- Plantar flexor spindle reflex gains during the stance (st) and swing (sw) phases, KS^{st} and KS^{sw}: these parameters are evaluated with increased values to model spastic hyperreflexia and reduction of presynaptic inhibition. KS^{st} is also evaluated with decreased values to model neural weakness. By contrast, KS^{sw} is not evaluated with decreased values as plantar flexor muscles are mainly activated during the stance phase.
- Plantar flexor length reflex gains during the stance and swing phases, KL^{st} and KL^{sw}: these parameters are similarly evaluated with increased values to reproduce hyperreflexia and KL^{st} is evaluated with reduced values to mimic neural weakness.
- Plantar flexor force reflex gain during the stance phase, KF^{st}: this parameter is evaluated with both increased and decreased values to reproduce hyperreflexia and neural weakness, respectively.
- TA to plantar flexor spindle reflex gains during the stance and swing phases, KS_{TA}^{st} and KS_{TA}^{sw}: as these reciprocal reflexes are negative, their gains are evaluated with decreased absolute values corresponding to increased real values to reproduce a reduction of reciprocal inhibition. Further, positive gains mimic reciprocal facilitation that abnormally excites antagonist muscles after switching from reciprocal inhibition to facilitation.

Generation and automation of pathological optimisations

Each parameter alteration of interest detailed above is individually induced in the model for a range of altered values, resulting in a gait without fall after optimisation. To do so, we define a broad range of altered values as a percentage of the corresponding healthy optimisation value. We set the altered values to both SOL and GAS of both legs for a biomechanical or reflex parameter. In this last case, the reflex parameter is fixed and will not be optimised. Meanwhile, the variation of the remaining reflex parameters is constrained. Some impairments occur gradually along with neural adaptations such as in CP, whereas other impairments can be sudden, for instance after stroke or SCI. Compensation through neural adaptations may also arise in these pathological conditions, especially after training (Knikou, 2010; Smith et al., 2015). Nevertheless, such adaptations are difficult to study through simulation as we do not know the cost function in pathological conditions. Minimisation of the effort might play a minor role compared to healthy conditions, whereas pain, which is difficult to compute, might play a more important role for instance.

	Stance			Swing	
	ES	MS	PS	S	LP
GMAX	PD+, C		C	F+	
HAMS	PD+, C			F+	
ILPSO	PD-, C		C	L+, L- (HAMS)	
VAS	C, F+				
SOL	F+, L+, V+			F-, L+, V+	
	V- (TA)			V- (TA)	
GAS	F+, L+, V+			F-, L+, V+	
	V- (TA)			V- (TA)	
TA	L+, V+			L+, V+	
	F- (SOL)				

Figure 4. Extended gait controller from Geyer and Herr
The additional SOL, GAS and TA direct and reciprocal reflexes are indicated in blue. For instance, S_+ means a positive direct spindle reflex from the muscle to itself, whereas S_{-TA} means a negative reciprocal spindle reflex from the TA to the muscle. [Colour figure can be viewed at wileyonlinelibrary.com]

The goal is here to systematically study the strict and short-term effect of various individual impairments on gait (and therefore to stay close to the healthy parameter values, except for the altered parameters). The remaining reflex parameters are thus set to the corresponding healthy optimisation values with a limited variation of 5% allowed for the optimiser to act upon. Each parameter is drawn from a Gaussian distribution characterised by its mean and standard deviation (SD). Furthermore, each parameter is also upper and lower bounded to reject parameters outside a permissible range. Thus, to constrain a parameter from varying from baseline, we set its upper and lower boundaries with a small SD from the healthy optimisation results. For biomechanical parameter alterations, optimisations are run with all the reflex parameters set to their healthy optimisation value with a limited variation of 5% (with smaller limited variations, optimisations could not reach gaits without fall for small alterations). We apply this strategy to limit potential compensation from other muscle reflexes while at the same time offering some flexibility that allows optimisations to reach gaits without fall.

We adapt the cost functions used for optimising the healthy gait by considering a lower minimal speed set to 0.5 m/s and larger joint ranges for the joint measure. Each extremum is more precisely set to two times the previous extremum, leading to the following ranges: for the pelvis, hip and ankle respectively: $[-30°, 15°]$ for the pelvis retroversion–anteversion, $[-40°, 80°]$ for the hip extension–flexion and $[-60°, 30°]$ for the plantarflexion–dorsiflexion. Each of these pathological optimisations is then run over 500 iterations. Here we do not define any specific stopping condition, but we limit the number of iterations to reach a gait without immediate fall. If an optimisation does not reach such a gait (i.e. if the simulation falls immediately without taking 12 steps), we do not consider the corresponding altered value.

The optimisation method introduces randomness in the initial conditions and parameters so that the population of solutions tends to lead to similar conclusions. To further check the repeatability of our results, we run several optimisation trials with various initial conditions (IC) for some of the altered parameters. We consider the IC we use for the results presented above and modify each joint by $+10$ or $-10°$. We number these various IC from 1 to 6 with $IC1$ the IC used for the main results, $IC2$ the same IC with the right hip with $+10°$, $IC3$ with the right knee with $-10°$, $IC4$ with the right ankle with $+10°$, $IC5$ with the left knee with $-10°$ and $IC6$ with the left ankle with $+10°$. Then for each IC, we compute the mean absolute error between the mean ankle angle over the gait cycle and the mean ankle angle over the gait cycle of $IC1$ ($MAE_{IC1}\alpha$). Moreover, we compute the mean relative error between the optimised parameters and the optimised parameters of $IC1$ ($MRE_{IC1}p$). Thus, we can

check if the various optimisation trials result in similar results in terms of kinematics and parameter values.

Finally, we further this one-dimensional (1D) exploration by a two-dimensional (2D) exploration in which some reflex parameters are investigated together (see some examples below). We determine the pairs of parameters of interest later according to the results of the 1D exploration. Optimisations are similarly run with the values of two parameters altered simultaneously, and limited variation is allowed on the remaining ones. The previous 1D exploration ranges define the 2D space of altered values.

Pathological gait characterisation

All these parameter alteration evaluations result in simulated gaits that need to be characterised as pathological or not. Toe walking is characterised by an excessive ankle plantarflexion throughout the stance phase, an absence of the first ankle rocker, an early third ankle rocker and a predominant early ankle plantarflexion moment (Alvarez et al., 2007). The first and third ankle rockers correspond to the ankle plantarflexion movements respectively from heel-strike to flat foot on the ground at the beginning of the stance phase, and from heel-off to toe-off at the end of the stance phase (Brockett & Chapman, 2016). Severe toe gaits present all the previous deviations, whereas mild to moderate toe gaits do not present a predominant early ankle plantarflexion moment nor necessarily rocker deviations (Alvarez et al., 2007). Heel walking is characterised by an increased slope towards dorsiflexion or a dorsiflexion peak $>20°$ (Nieuwenhuys et al., 2015), and a reduced ankle plantarflexion moment during the stance phase (Lamontagne et al., 2002). Each simulated gait contains about 12 gait cycles that may present variability. To consider this variability while distinguishing initial transitions depending on initial conditions from steady-state behaviour (the steady states can show variability), we compute each metric described below on each gait cycle except the first one and compute their mean and SD. Thus, we define the following metrics based on ankle kinematics and ankle moment to characterise simulated gaits.

Ankle kinematics comparison. For each investigated parameter, we plot the mean hip, knee and ankle angles (ankle angle is noted α) over the gait cycles of each altered value. We extract and normalise each gait cycle to gait cycle percentage ($[0, 100]\%$). Then, we interpolate each gait cycle joint angle on the mean gait cycle and average the joint angles over the gait cycles. We similarly plot the mean joint angles of the healthy optimisation (healthy ankle angle is noted α_h). Thus, we can compare the effect of the alterations on the ankle profile, and in particular

on the ankle rockers. The initiation time of the third ankle rocker is computed from the ankle velocity when it takes a null value. Based on Alvarez et al. (2007), we consider a simulated gait as toe gait if the third ankle rocker occurs before 30% of the gait cycle, compared to healthy gait presenting a third ankle rocker at the end of the stance phase (after 40% of the gait cycle). We name this criterium $C_{toe}1$.

For each simulation, we also compute the mean and the maximum ankle angle ($\bar{\alpha}$ and α_{max}) during each MS and PS period that we hereafter name ST (ST = MS + PS):

$$\begin{cases} \bar{\alpha}^{ST} = \frac{1}{N_{ST}} \sum_{n \in ST} \alpha_n^{ST} \\ \alpha_{\max}^{ST} = max_{n \in ST} \left(\alpha_n^{ST} \right) \end{cases} \qquad (6)$$

with N_{ST} the number of ST samples. The mean and SD of $\bar{\alpha}^{ST}$ and $\alpha_{\max}^{ST}$ over the gait cycles are finally computed. Based on Nieuwenhuys et al. (2015), we consider a simulated gait as heel walking if $\alpha_{\max}^{ST}$ is >20°. We name this criterium $C_{heel}1$.

The simulation mean ankle angle estimates $\bar{\alpha}^{ST}$ are first compared with reported ankle angles during pathological gaits. For instance, several studies analysed the gait of CP children and provided experimental ankle angle measures, but with large intra- and inter-study variability as patient conditions can be widely different (Granata et al., 2000; Kerkum et al., 2015; Papadonikolakis et al., 2003). Moreover, our simulations fall before reaching severe pathological gaits (because our models do not incorporate sophisticated balance control). Therefore, as the goal here is to investigate the effect of the altered parameters on gait simulation, we consider our healthy optimisation as reference and the kinematics features based on the method used by Schwartz et al. (2008) to identify gait deviations. According to this identification system, plantarflexion (respectively dorsiflexion) is excessive during the stance phase if $\bar{\alpha}^{ST} < \bar{\alpha}_{ref}^{ST} - std(\bar{\alpha}_{ref}^{ST})$ (respectively $\bar{\alpha}^{ST} > \bar{\alpha}_{ref}^{ST} + std(\bar{\alpha}_{ref}^{ST})$ with α_{ref} a healthy reference. Based on the experimental healthy ankle angle with a mean SD of 3.5° during the stance phase reported by Schwartz et al. (2008), we thus consider a simulated gait as toe or heel walking if $\Delta_h \bar{\alpha}^{ST} = \bar{\alpha}^{ST} - \bar{\alpha}_h^{ST}$ is lower than −3.5° or larger than 3.5°, respectively. We name these criteria $C_{toe}2$ and $C_{heel}2$.

Ankle moment comparison. We similarly plot the mean normalised ankle moment (M) over the gait cycles of each altered value for each parameter of interest. Then, we compute the mean and SD of the mean ankle moment during the stance phase ($\bar{M}^{ST}$) for each simulated gait to characterise heel gait. Similarly to the comparison of ankle kinematics, we consider the healthy ankle moment SD during the stance phase reported by Schwartz et al. (2008), 0.19 Nm/kg, and characterise a simulated gait as

heel walking if $\Delta_h \bar{M}^{ST} = \bar{M}^{ST} - \overline{M_h}^{ST}$ is >0.19 Nm/kg. We name this criterium $C_{heel}3$.

Moreover, toe gait can present a predominant early ankle moment peak, whereas in healthy gait, the ankle moment increases throughout the beginning of the stance phase (Alvarez et al., 2007). Thus, we also compute the difference between the ankle moment peak during the ST period and the eventual peak during the ES period. If there is no moment peak during the ES or the ST period, we consider the maximum of the moment during the period:

$$\Delta M_{peaks} = max \left(M^{ST} \right) - max \left(M^{ES} \right) \qquad (7)$$

We finally characterise a simulated gait as toe walking if ΔM_{peak} is negative according to Alvarez et al. (2007). We name this criterium $C_{toe}3$.

Thus, we take account of several criteria to characterise pathological toe and heel gaits and we consider a simulated gait as toe or heel gait if all these criteria are fulfilled. If some of them are satisfied but not all, we consider the simulated gait as partial toe or heel gait.

Statistical treatment of the data. As detailed above, each simulated gait contains about 12 gait cycles. For each simulation, we compute the various metrics described above on each gait cycle except the first one and compute their mean and SD.

Results

This section first presents the healthy gait resulting from the optimisation of our new reflex circuit model. We compare the simulation estimates of the pelvis tilt, hip, knee and ankle angles and moments, and ground reaction forces to healthy experimental data ranges. We also compare muscle activations of the healthy optimisation to experimental EMG timings. To further evaluate this healthy result, we analyse the optimised reflex gains with respect to pathway modulations during gait reported in the literature.

Simulations of altered biomechanical parameters are then outlined, followed by simulations of altered reflex parameters. All these results are tabulated and those leading to pathological gaits are analysed in more detail with the ankle kinematics and moment comparison. All the results are presented for the left leg (l).

Healthy optimisation

The optimisation of our new reflex circuit model (i.e. Geyer and Herr's model extended with additional reflexes) results in a healthy gait that can be visualised

following the link provided in the Additional information section. Snapshots of the simulation are also presented in Fig. 5*A*.

The resulting walking speed and step length are respectively 1.16 m/s and 0.8 m. The quality of this simulated gait is first evaluated through analysis of its joint angles and moments, ground reaction forces and muscle activation estimates. This gait analysis is presented in Fig. 6. The simulation states of joint angles and

moments, and ground reaction forces are plotted with healthy experimental data ranges reported by Schwartz et al. (2008). This gait analysis shows regular pelvis tilt, hip flexion, knee angles and moments, and ground reaction forces. The ankle angle reproduces the experimental profile with a less pronounced plantarflexion at the push-off phase and slightly excessive dorsiflexion at the gait cycle transition. The third ankle rocker occurs well after 40% of the gait cycle, as reported in the literature
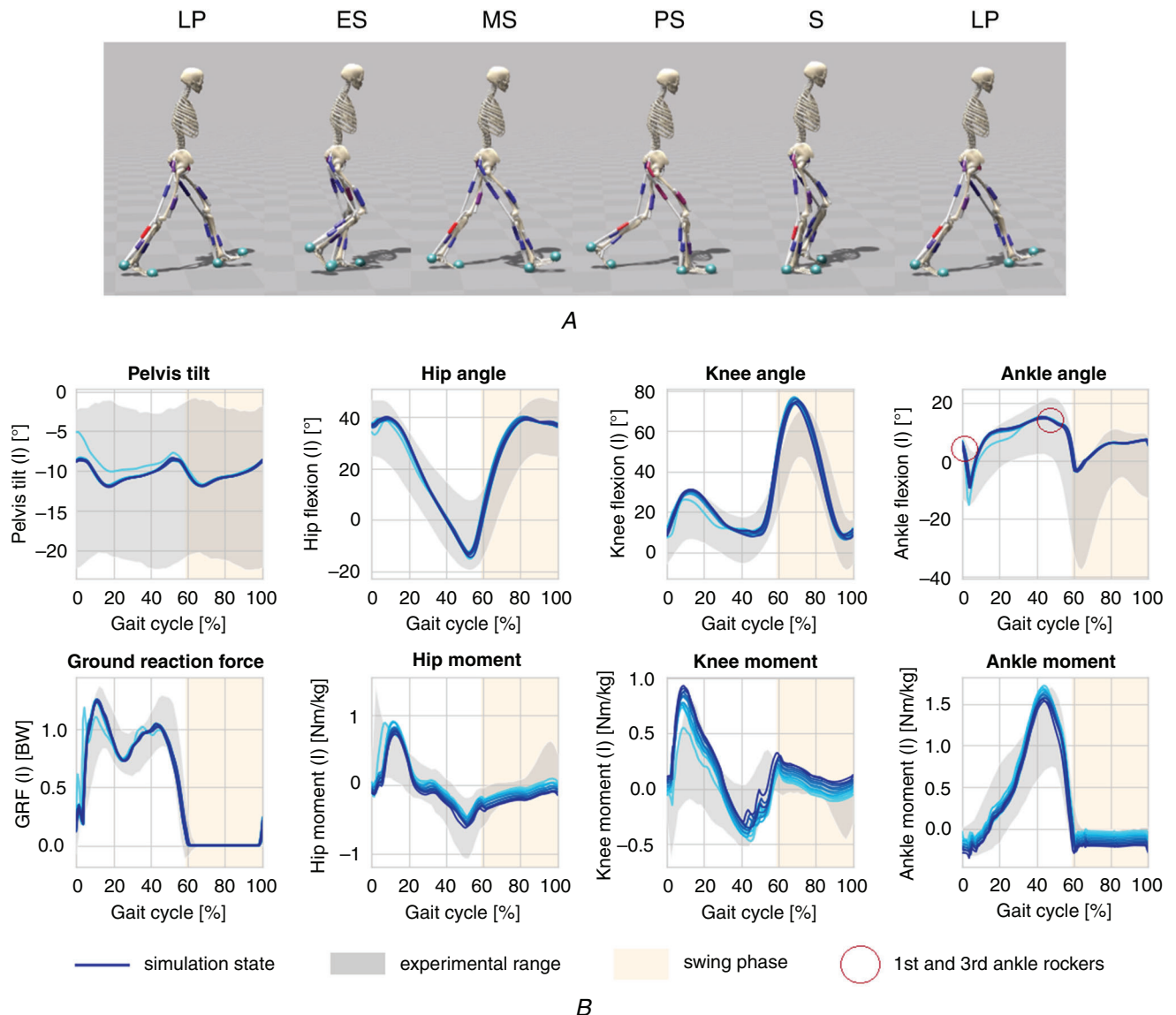

Figure 5. Healthy reflex circuit model optimisation
A, snapshots of the optimised healthy gait at the beginning of each controller state: LP, ES, MS, PS, S and LP. *B*, gait analysis: simulation states of the pelvis tilt, hip, knee and ankle angles and moments, and ground reaction forces over the gait cycles are compared with healthy experimental data ranges reported by Schwartz et al. (2008) ($\mu \pm 2 * std$) in grey. Curves from cyan to blue correspond to the 11 simulated gait cycles. The optimisation result shows regular states. The ankle angle reproduces the experimental profile with a less pronounced plantarflexion at the push-off phase and slightly excessive dorsiflexion at the gait cycle transition. The first and third rockers are circled in red. The knee flexion and moment also show excessive values at the beginning of the swing and stance phase, respectively. [Colour figure can be viewed at wileyonlinelibrary.com]

Table 1. Optimised values of SOL, GAS and TA direct and reciprocal reflex gains during the stance and swing phases

Phase	Parameter							
	KS_{SOL}	KS_{GAS}	KL_{SOL}	KL_{GAS}	KF_{SOL}	KF_{GAS}	KS_{TA-SOL}	KS_{TA-GAS}
Stance	0.16	0.17	4.0	0.08	0.23	1.4	−0.85	−0.34
Swing	0.11	0.26	0.80	0.01	−0.91	−1.8	−3.3	−1.7

(Alvarez et al., 2007). The knee flexion and moment also show excessive values at the beginning of the swing and stance phase respectively. In comparison, Geyer and Herr's results show an ankle flexion profile that better reproduces experimental data, whereas Ong's results also show excessive dorsiflexion throughout the gait cycle. Geyer and Herr's results show better matching ankle kinematics, which may result from the fact that their model has fewer parameters than ours or Ong's. Parameter fine-tuning to minimise the cost function may then be easier.

Furthermore, similarly to Ong et al. (2019), Fig. 6 compares the muscle activations of this healthy optimisation to experimental EMG on–off timings reported by Perry and Burnfield (2010a). The timings of simulation states match the experimental ones correctly, except for ILPSO at the beginning of the stance phase and VAS at the end of the swing phase. Such muscle inactivity is also present in Geyer and Herr's and Ong's results. This

figure also shows a larger activation of GAS compared to SOL during the stance phase.

The optimised values of SOL, GAS and TA reflex gains are also presented in Table 1. They highlight the following major modulations during gait that are in line with the literature:

- SOL spindle reflex gain is larger during the stance phase compared with the swing phase. This difference corresponds to the modulation of the stretch reflex that occurs between stance and swing phases (Faist et al., 1995). The stretch reflex indeed participates in propulsion during the stance phase and stabilisation during both stance and swing phases (Zehr & Stein, 1999). Regarding the GAS muscle, its spindle reflex gain is larger during the swing phase compared with the stance phase. As the GAS muscle is also involved in knee flexion (bi-articular muscle), it is reasonable that the modulation of its stretch reflex is different.
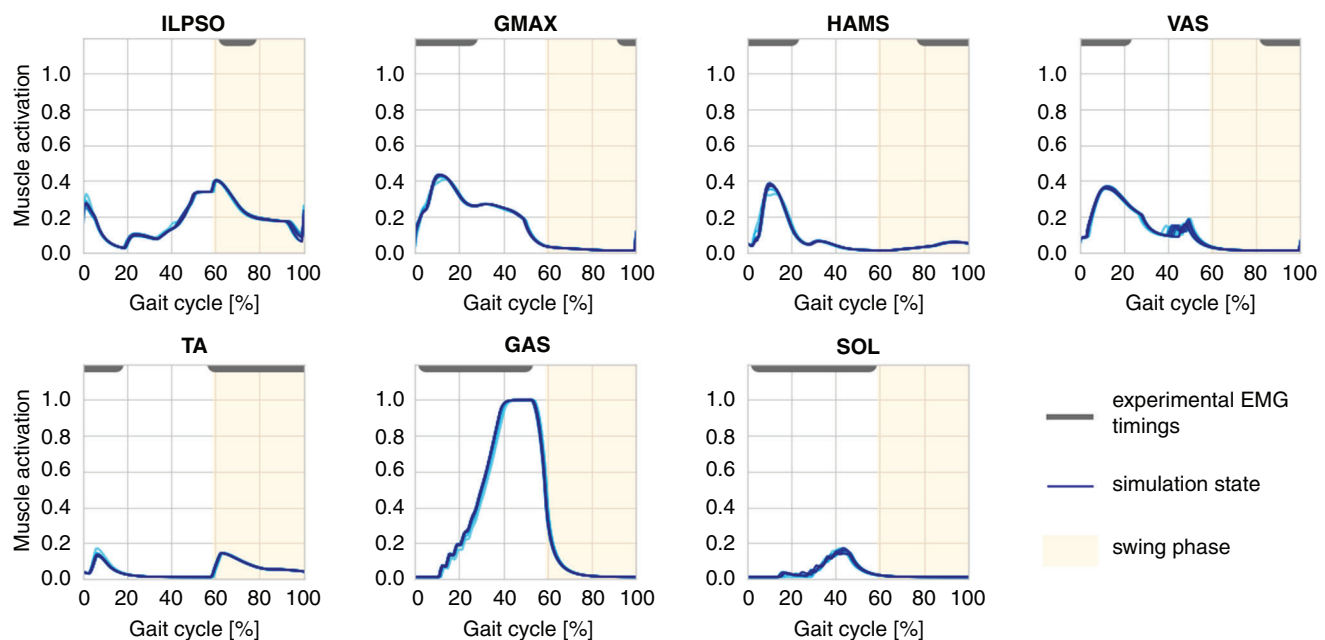
Figure 6. Muscle activations of the healthy optimisation over the gait cycles
The simulation states are compared to experimental EMG on–off timings in grey reported by Perry and Burnfield (2010a). Curves from cyan to blue correspond to the 11 simulated gait cycles. The timings of the simulation and experimental data match correctly, except for ILPSO at the beginning of the stance phase and VAS at the end of the swing phase. [Colour figure can be viewed at wileyonlinelibrary.com]

Table 2. Plantar flexor biomechanical parameter alterations and pathological gaits

Parameter	Evaluated values as percentage of the healthy value	Partial toe gait range (some toe gait criteria are fulfilled, but not all)	Partial heel gait range (some heel gait criteria are fulfilled, but not all)	Falling threshold
F_{max}	90, 80…60%	Ø	$C_{heel}1$ and $C_{heel}3$, but not $C_{heel}2$: [70, 60]%	50%
l_0^{fib}	95, 90%	$C_{toe}1$ and $C_{toe}2$, but not $C_{toe}3$: 90%	Ø	85%

This table outlines the evaluation of biomechanical parameters. For each, the evaluated values are provided as a percentage of the healthy value. The eventual range leading to toe gait (some toe gait criteria are fulfilled, but not all) and the eventual range leading to partial heel gait (some heel gait criteria are fulfilled, but not all) are also provided as a percentage of the healthy value. Ø indicates that any parameter alteration leads to toe or heel gait before the falling threshold. The falling threshold corresponds to the parameter value at which the simulation falls immediately. If the simulation does not fall in the range of values of the parameter evaluation, the possible falling threshold beyond this range is indicating with the symbol $>$ or $<$. Thus, reduced F_{max} mimicking muscle weakness induces partial heel gait, whereas reduced l_0^{fib} reproducing muscle contracture induces partial toe gait.

- TA to plantar flexor spindle reflex gains are smaller during the swing phase compared with the stance phase. As these reciprocal reflexes are negative, this difference corresponds to the reciprocal stretch inhibition between stance and swing phases. Thus, these reciprocal reflexes participate in inactivation of the antagonist muscles in the appropriate phases of the gait cycle. Here, TA inhibits the plantar flexors during the swing phase to avoid plantarflexion (Petersen et al., 1999).

Pathological optimisations

Biomechanical impairments. Figure 7 compares the simulated gait resulting from reduced plantar flexor F_{max} to 60%, mimicking muscle weakness with the healthy gait. The corresponding simulation can also be visualised
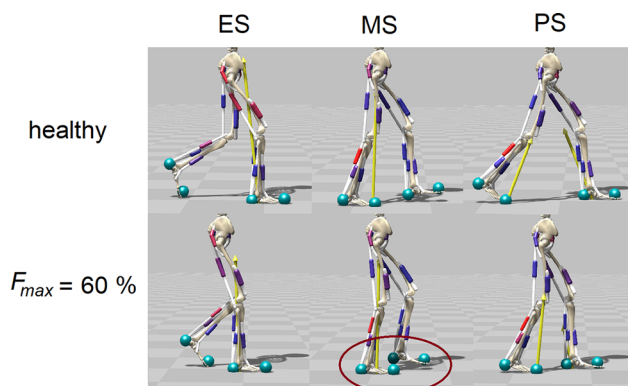

Figure 7. Comparison of the gait resulting from reduced plantar flexor F_{max} to 70% mimicking muscle weakness with the healthy gait: snapshots during ES, MS and PS phases
The yellow arrows represent ground reaction forces. There is a smaller step length in the altered condition compared to the healthy one, but no significant larger dorsiflexion characterising heel gait. [Colour figure can be viewed at wileyonlinelibrary.com]

following the link provided in the Additional information section. We can see that the altered condition induces a smaller step length, but no severe increase in dorsiflexion. The effect of reduced F_{max} on gait is further presented in Fig. 8. The ankle kinematics and moment comparison highlight large dorsiflexion and reduced plantarflexion moment during the late stance period compared with a healthy gait. The corresponding α_{max}^{ST} and $\Delta_h \bar{M}^{ST}$ metrics fulfil the criteria $C_{heel}1$ and $C_{heel}3$ ($\alpha_{max}^{ST} > 20°$ and $\Delta_h \bar{M}^{ST} < -0.19$ Nm/kg, respectively), but the $\Delta_h \bar{\alpha}^{ST}$ metric does not reach values characterising heel gait (criterium $C_{heel}2$, $\Delta_h \bar{\alpha}^{ST} > 3.5°$).

Table 2 summarises the two biomechanical parameter alterations investigated in this study. Reduced l_0^{fib} reproducing muscle shortening induces toe gait only partially. Early plantarflexion during the stance phase corresponding to a fulfilled criterium $C_{toe}1$ can still be observed in the ankle kinematics comparison. Moreover, this parameter is noticeably sensitive, with small alterations leading to model falling.

Neural impairments. Figure 9 compares the simulated gait resulting from increased plantar flexor KS^{ST} to 400%, mimicking hyperreflexia with the healthy gait. We can observe that only the toes touch the ground during the MS phase in the altered condition as in typical toe gait. The effect of increased KS^{ST} on the ankle angle and moment is further presented in Fig. 10. The ankle kinematics comparison highlights early and large plantarflexion during the stance phase characterising toe gait (3rd ankle rocker before 30% of the gait cycle and $\Delta_h \bar{\alpha}^{ST} < 3.5°$ corresponding to criteria $C_{toe}1$ and $C_{toe}2$). The moment comparison also shows predominant early plantarflexion moment peaks characterising toe gait ($\Delta M_{peaks} < 0 Nm/kg$ corresponding to criterium $C_{toe}3$). The knee kinematics comparison also reveals a larger knee flexion during the stance phase.

Table 3 summarises all the reflex parameter alterations investigated in this study. Increased plantar flexor F reflex gain mimicking hyperreflexia during the stance phase similarly induces toe gait. Increased KS_{TA}^{st}, corresponding to decreased absolute values, reproduce a reduction of reciprocal inhibition and also lead to toe gait. The effects of increased KF^{st} and KS_{TA}^{st} on gait are similar to those of KS^{st}. Corresponding simulations can also be visualised following the link provided in the Additional information section.

By contrast, increased KL^{st} and reflex gains during the swing phase do not induce toe gait. Early plantarflexion during the stance phase can still be observed for KL^{st} increases (criteria $C_{toe}1$ and $C_{toe}2$ are fulfilled, but not $C_{toe}3$), whereas increases in reflex gains during the swing phase do not have significant effects on the gait kinematics. Alterations of plantar flexor reflex parameters during the stance phase thus have greater effects on gait compared to parameters during the swing phase.

Regarding decreased reflex gains reproducing neural weakness, they induce partial heel gait in a similar way

to muscle weakness. KS^{st} and KF^{st} are also sensitive parameters when reduced as l_0^{fib}.

Finally, the qualitative effect of all evaluated biomechanical and reflex parameter alterations on gait is summarised in Fig. 11.

Repeatability of the results. Figure 12 presents the results of various optimisation trials for the maximal isometric force altered to 70% and the stance spindle gain altered to 300% with various IC. These results show similar ankle kinematics and optimised parameter values for the various IC (small $MAE_{IC1}\alpha$ and $MRE_{IC1}p$) arguing for the repeatability of our results.

2D exploration. The previous 1D exploration is furthered by a 2D exploration of some pairs of reflex parameters of interest. As hyperreflexia usually occurs during both stance and swing phases, plantar flexor hyperreflexia is first modelled during both phases through KS and KL reflex gains. The investigation of neural weakness is
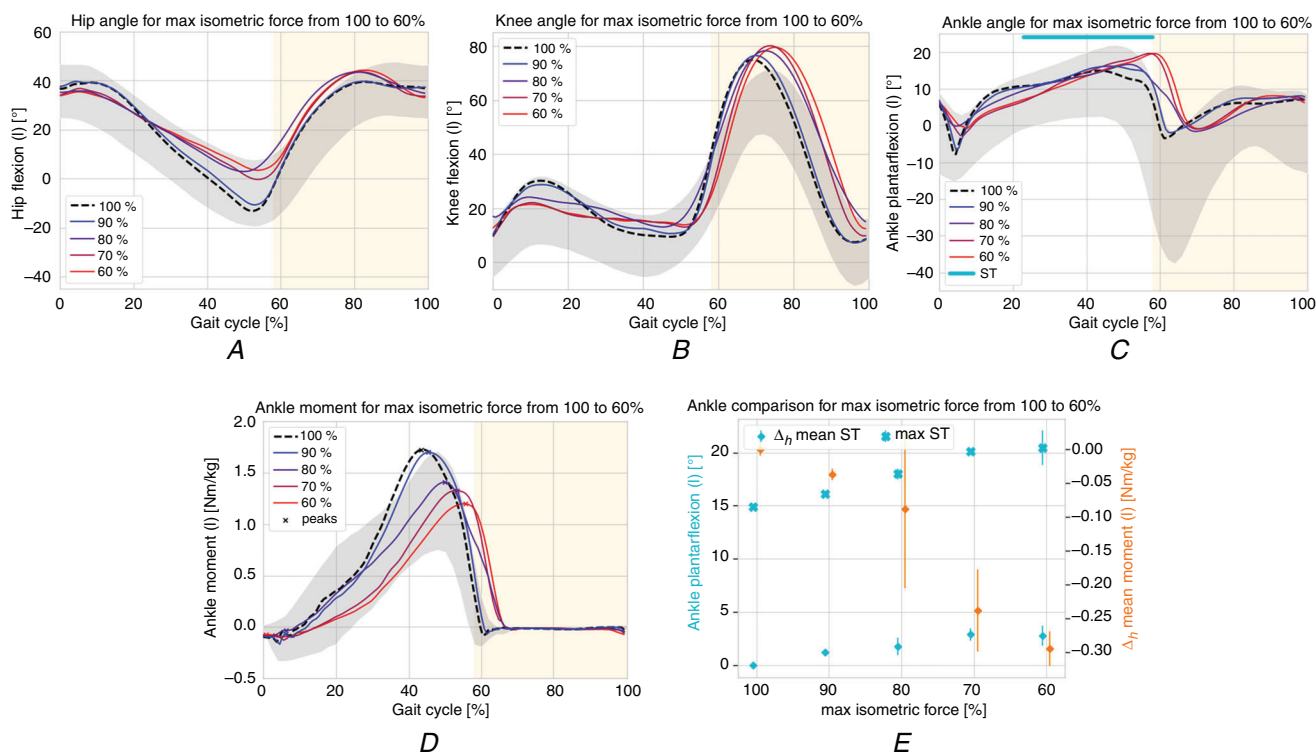

Figure 8. Effect of reduced plantar flexor maximal isometric force (F_{max}) mimicking muscle weakness on gait

A, hip angle (l) for plantar flexor F_{max} from 100 to 70%: the grey area represents healthy experimental data range reported by Schwartz et al. (2008) ($\mu \pm 2 * std$) and the light orange area indicates the healthy swing phase. *B*, similar knee angle. *C*, similar ankle angle: alterations lead to large dorsiflexion during the late stance period. The ST period over which $\Delta_h \tilde{\alpha}^{ST}$ and α_{max}^{ST} are computed is indicated by the cyan top line. *D*, similar ankle moment with the moment peaks indicated by crosses: alterations reduce plantarflexion moment during the late stance period. *E*, corresponding $\Delta_h \tilde{\alpha}^{ST}$, α_{max}^{ST} and $\Delta_h \bar{M}^{ST}$. [Colour figure can be viewed at wileyonlinelibrary.com]

Table 3. Reflex parameter alterations and pathological gaits

Parameter	Evaluated values as percentage of the healthy value	Toe gait range (tThe three toe gait criteria are fulfilled)	Partial heel gait range (some heel gait criteria are fulfilled, but not all)	Falling threshold
KS^{st}	150, 200…400%	[250, 400]%	Ø	450%
	95, 90…75%	Ø	$C_{heel}1$ and $C_{heel}2$, but not $C_{heel}3$: 75%	70%
KS^{sw}	150, 200…450%	Ø	Ø	500%
KL^{st}	150, 200…450%	Ø	Ø	500%
	90, 80…40%	Ø	$C_{heel}1$ and $C_{heel}3$, but not $C_{heel}2$: 40%	30%
KL^{sw}	200, 300…700%	Ø	Ø	800%
KF^{st}	200, 300…900%	[300, 900]%	Ø	>900%
	95, 90…80%	Ø	$C_{heel}1$ and $C_{heel}3$, but not $C_{heel}2$: 80%	75%
$KS_{TA}{}^{st}$	90, 80…20%	[70, 20]%	Ø	10%
$KS_{TA}{}^{sw}$	90, 80…10%	Ø	Ø	0%

This table outlines the evaluation of parameters from the reflex circuit model with increased and decreased values. For each, the evaluated values are provided as a percentage of the healthy value. The eventual range leading to toe gait (the three toe gait criteria are fulfilled) and the eventual range leading to partial heel gait (some heel gait criteria are fulfilled, but not all) are also provided as a percentage of the healthy value. Ø indicates that any parameter alteration leads to toe or heel gait before the falling threshold. The falling threshold corresponds to the parameter value at which the simulation falls immediately. If the simulation does not fall in the range of values of the parameter evaluation, the possible falling threshold beyond this range is indicated with the symbol > or <. Thus, reduced F_{max} mimicking muscle weakness induces partial heel gait, whereas reduced $l_0{}^{fib}$ mimicking muscle contracture does not induce toe gait. Thus, increased F and S reflex gains mimicking hyperreflexia during the stance phase induce toe gait, whereas reduced reflex gains mimicking neural weakness do not induce heel gait.

similarly extended by reducing both KF and KL reflex gains during the stance phase. The results of these 2D explorations are presented through colour maps of the ankle kinematics and moment metrics, $\Delta_h\bar{\alpha}^{ST}$, α_{max}^{ST} and ΔM_{peaks}. Plantar flexor hyperreflexia thus lead to more pronounced toe gait and neural weakness to more pronounced heel gait. Simulations can also be visualised following the link provided in the Additional information section.

Figure 9. Comparison of the gait resulting from increased plantar flexor KS^{st} to 400% mimicking hyperreflexia with the healthy gait: snapshots during ES, MS and PS phases
The yellow arrows represent ground reaction forces. As in typical toe gait, only the toes touch the ground during the MS phase in the altered condition. [Colour figure can be viewed at wileyonlinelibrary.com]

Figure 13A and C show smaller $\Delta_h\bar{\alpha}^{ST}$ and ΔM_{peaks} corresponding to more pronounced toe gaits induced by increased plantar flexor KS during both stance and swing phases compared to 1D exploration results. TA to plantar flexor KS and plantar flexor KL increases during the two phases also lead to more pronounced toe gait. These results also highlight further the main effect of increased reflex gains during the stance phase.

Similarly, Fig. 13B and D show larger α_{max}^{ST} and smaller ΔM_{peaks}, and therefore more pronounced heel gaits induced by plantar flexor KF and KL reduction during the stance phase compared to 1D exploration results.
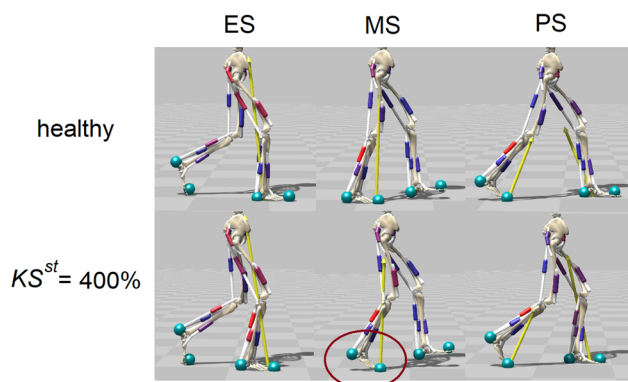
Discussion

This investigation of the effect of both biomechanical and neural impairments on gait is based on a reflex circuit model including plantar flexor force, spindle and length direct pathways, and additional reciprocal pathways with TA. We model pathways that were omitted by previous models to extend our investigation. Optimisation of this reflex circuit model results in a healthy gait model highlighting reported pathway modulations during gait. We then investigate the effect of plantar flexor SOL and GAS impairments from both biomechanical and neural origins. We explore the effect of each impairment while constraining the variation of the other parameters in order to study the strict and short-term effect on gait. On the one

hand, toe gaits can be generated by increased spindle and force reflex gains modelling spastic hyperreflexia during the stance phase. These results reproduce both clinical observations (Armand et al., 2016; Chia et al., 2020) and previous simulations. In particular, they are comparable to Jansen et al.'s (2014) simulation that reproduces excessive plantarflexion with increased length and velocity feed-backs, and lack of suppression of the stretch reflex of plantar flexor muscles during the swing phase. Increased

spindle reciprocal pathways from the TA to the plantar flexors reproducing reduction of reciprocal inhibition also lead to toe walking. These reflex increases modelling hyperreflexia coherently simulate toe gait. Moreover, these simulations of plantar flexor hyperreflexia reveal excessive knee flexion during the stance phase. This gait deviation corresponds to the pathological crouch gait that is also commonly present in CP and, in part, attributed to plantar flexor spasticity (Armand et al., 2016; James et al., 2009).
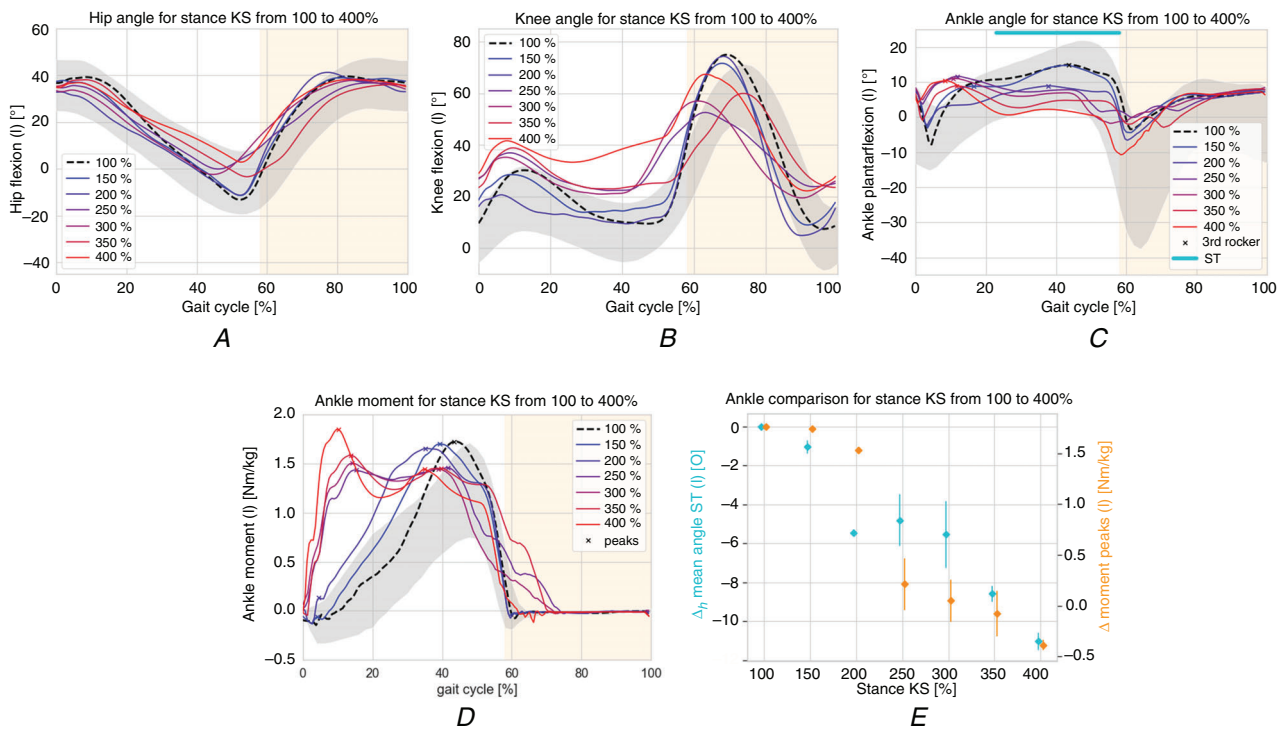

Figure 10. Effect of increased plantar flexor stance KS (KS^{st}) mimicking hyperreflexia on gait
A, hip angle (l) for plantar flexor KS^{st} from 100 to 400%: the grey area represents healthy experimental data range reported by Schwartz et al. (2008) ($\mu \pm 2 * std$) and the light orange area indicates the healthy swing phase. *B*, similar knee angle: alterations lead to larger knee flexion during the stance phase. *C*, similar ankle angle with the 3rd ankle rocker initiations indicated by crosses: alterations lead to early and large plantarflexion during the stance phase. The ST period over which $\Delta_h \bar{\alpha}^{ST}$ is computed is indicated by the cyan top line. *D*, similar ankle moment with the moment peaks indicated by crosses: alterations induce predominant early plantarflexion moment peaks characterising toe gait. *E*, corresponding $\Delta_h \bar{\alpha}^{ST}$ and ΔM_{peaks}. [Colour figure can be viewed at wileyonlinelibrary.com]

Figure 11. Qualitative effect of every evaluated plantar flexor biomechanical and reflex parameter alterations on gait
Increased and decreased values are represented by > and < symbols, respectively. As $KS_{TA}{}^{st}$ is negative, it is evaluated with decreased absolute values corresponding to increased real values to reproduce reduction of reciprocal inhibition. Induced toe gait is highlighted in red, whereas induced large plantarflexion and dorsiflexion during the stance phase are shown in light red and light blue, respectively. [Colour figure can be viewed at wileyonlinelibrary.com]

On the other hand, other impairments that were expected to generate pathological gaits only partially do so (some criteria are fulfilled, but not all). First, regarding biomechanical impairments, reduced maximal isometric force modelling muscle weakness induces partial heel gait, whereas reduced optimal fibre length reproducing muscle contracture results in partial toe walking. Reduced optimal fibre length still induces early ankle plantarflexion, whereas reduced maximal isometric force leads to large dorsiflexion mainly during the late stance period corresponding to a weak propulsion of the body. In comparison, Ong et al. (2019) simulate heel and toe walking by modelling SOL and GAS weakness and contracture respectively. However, the corresponding optimised reflex parameters are not constrained to a small range around the healthy value as in the present study. Ong et al. (2019) also reproduce toe walking by modelling contracture to the SOL only. We considered

alterations to the properties of both plantar flexors as they are agonist muscles and are commonly impaired simultaneously. Nevertheless, they do not have the exact same role (Attias et al., 2017; Lenhart et al., 2014), and Matjacic et al. (2006) showed that SOL and GAS contractures do not have the same effects on gait kinematics. Perry and Burnfield (2010b) also state that the main cause of heel gait is SOL weakness whereas GAS weakness does not directly contribute to excessive ankle dorsiflexion. The present study could thus be furthered by distinguishing the effect of SOL and GAS impairments on gait. On another note, plantar flexor weakness is also assumed to contribute to crouch gait (Steele et al., 2012). Nevertheless, similarly to Ong et al. (2019) and Waterval et al. (2021), our simulations of plantar flexor weakness do not induce such gait deviation, and thus do not support such a contribution of plantar flexor weakness in crouch gait.
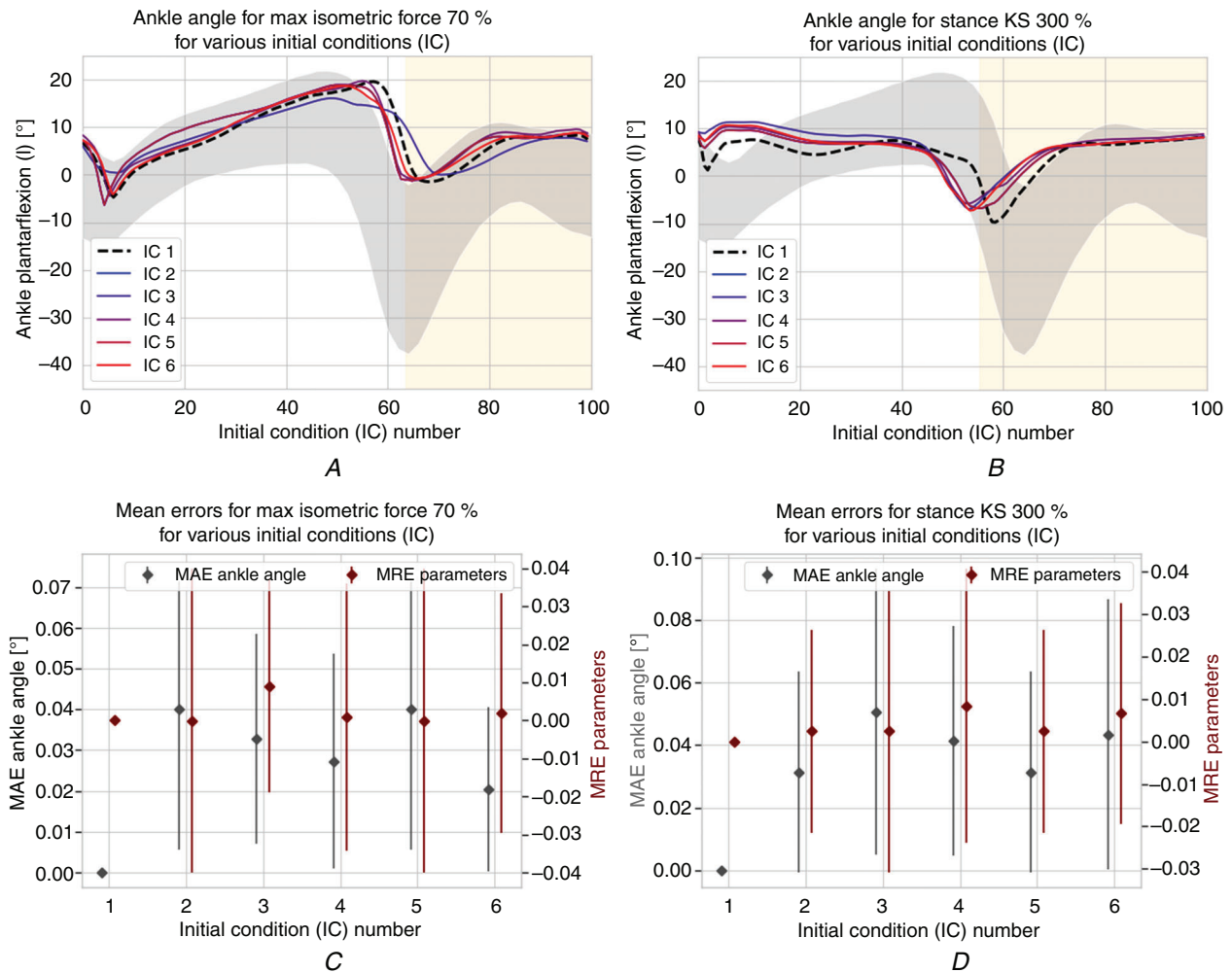

Figure 12. Repeatability of the results

A and *C*, various optimisation trials for the maximal isometric force altered to 70% with various IC: small $MAE_{IC1}\alpha$ and $MRE_{IC1}p$ indicate similar results. *B* and *D*, various optimisation trials for the stance spindle gain altered to 300%: small $MAE_{IC1}\alpha$ and $MRE_{IC1}p$ also indicate similar results. [Colour figure can be viewed at wileyonlinelibrary.com]

Regarding neural impairment, increased reflex gains during the swing phase do not result in toe gait. Alterations of plantar flexor reflex parameters during the stance phase thus have more effect on gait compared to parameters during the swing phase. The plantar flexor muscles are indeed mainly activated during the stance phase to propel the body forward. However, decreased plantar flexor reflex gains during the stance phase mimicking neural weakness induce partial heel gait. Furthermore, investigation of both hyperreflexia and neural weakness through 2D exploration reproduce more pronounced toe and heel gaits.

The present investigation is limited by the fact that the model falls before reaching severe pathological gait. Nonetheless, the sensitivity and the effect of parameter alterations towards plantarflexion or dorsiflexion can be observed. These results are significant because the contributions of active reflex pathways and passive muscle properties in spastic stiffness can barely distinguished in clinical examination (Lorentzena et al., 2010). Previous studies assumed that spastic stiffness is mainly caused by passive muscle properties (Dietz & Sinkjaer, 2007). However, the contribution of active reflex mechanisms is being progressively considered and reported as significant
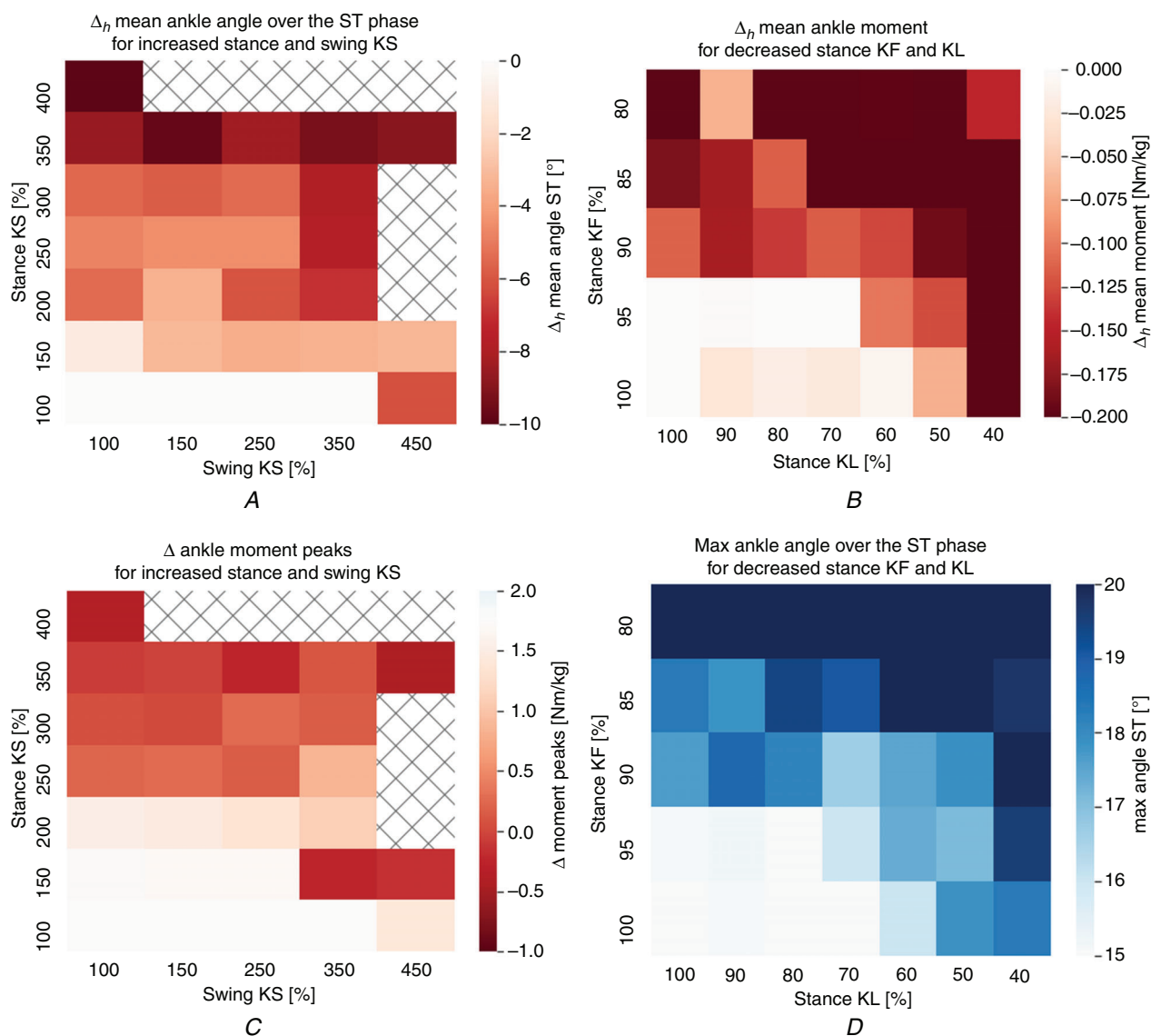

Figure 13. Effect of plantar flexor hyperreflexia and neural weakness on gait
A and *C*, effect of increased plantar flexor KS during both stance and swing phases: smaller $\Delta_h \tilde{\alpha}^{ST}$ and ΔM_{peaks} corresponding to more pronounced toe gait are induced compared to 1D exploration results. The checked squares indicate simulations that fall immediately. *B* and *D*, effect of reduced plantar flexor KF and KS during the stance phase: larger α_{max}^{ST} and smaller ΔM_{peaks} corresponding to more pronounced heel gait are induced compared to 1D exploration results. [Colour figure can be viewed at wileyonlinelibrary.com]

(Lorentzena et al., 2010; Mirbagheri et al., 2001). The present study suggests such an important contribution of active reflex mechanisms in pathological toe gait.

Nevertheless, the 'what if' approach applied in this study faces a major validation issue. On the one hand, we modelled numerous pathways that intrinsically lead to redundancy. The solution space may then contain several local minima. Given an optimised healthy gait state, our model predicts that specific pathways can elicit a pathology but our results might not generalise. In a different condition (e.g. faster or slower gait), this might not be true. However, the problem is difficult to explore as there are infinite possible initial conditions and parameters. The optimisation method still introduces randomness in the initial conditions and parameters (even for those constrained) so the population of solutions tends to lead to similar conclusions. To further argue for the repeatability of our results, we looked at suboptimal solutions and observed similar tendencies in both the gait kinematics and control parameter values. Furthermore, before impairing parameters we had already formed hypotheses on the different cause–effect relationship, which were confirmed when we observed agreement between simulation and clinical studies.

On the other hand, parameters are modified individually to investigate their effect on gait, but SCI, stroke or CP patients usually present many biomechanical and neural impairments together. Spasticity and muscle weakness can coexist in these conditions, leading to spastic paresis (Lamontagne et al., 2002). This study focuses on plantar flexors only, whereas these patients usually present multiple impaired muscles. Moreover, as mentioned previously, some impairments may be gradual along with progressive compensation through neural adaptations. Such adaptations may also arise after sudden impairments, especially after training. This topic of long-term adaptation and compensation is of great interest, but the state-of-the-art in pathological modelling is not at the point to address such complex conditions given that pathological gaits are by nature unstable. We plan to explore this topic in follow-up studies. Thus, validation of this study with clinical data is very challenging. This 'what if' approach is still deemed of great interest as one can postulate various hypotheses, then identify the conditions through simulation, and finally design an experiment that can help test and validate the model.

Besides its validation issue, this study could be improved on several points. First, the optimisation solution space could be further explored to look for other potential local minimums and reach a solution that better reproduces experimental observations. In particular, as outlined previously, knee angle and GAS activation present excessive values during the stance that could be refined. This exploration would require many optimisations that would take long to realise. More

sophisticated balance controllers could also be included to allow simulations to reach more severe pathological gaits. We also considered similar cost of function for healthy and impaired models, whereas human walking goals may vary depending on individual conditions. Minimisation of effort might play a minor role compared to healthy conditions, whereas pain might play a more important role for instance. Adapted measures for impaired optimisation could thus also be considered to reach more severe pathological simulations. On another note, more reflex parameters could be evaluated. Indeed, reflex offsets were not investigated, whereas their contribution to impaired motor control has been highlighted in the literature (Levin & Feldman, 1994). Neither were reflex delays evaluated, whereas increased delays are reported in SCI conditions for instance (Thomas et al., 2014). It should also be noted that the reflex pathway delays used in this study based on Geyer and Herr (2010) and Ong et al. (2019) are shorter than those recorded experimentally by the order of 50%. Moreover, even with delays closer to physiological values, a reflex-based controller is still only a first approximation of all the underlying neural pathways. The introduction of neuron models for afferent fibres, interneurons, alpha motor neurons and descending neurons would be a significant improvement to model in more detail descending pathways and presynaptic inhibition mechanisms, among others.

Conclusion

This study allows the targeting of various biomechanical and neural impairments leading to pathological gaits by simulating the effect of altered biomechanical and reflex parameters on gait. Our simulations suggest that toe walking can be generated by hyperreflexia, whereas muscle and neural weakness lead partially to heel gait. This 'what if' approach based on neuromusculoskeletal simulation is thus deemed of great interest and suggests an important contribution of active reflex mechanisms in pathological toe gait. Further modelling and simulation are essential to understand the cause–effect relationship between impaired mechanisms and pathological gaits in more detail. In this way, such neuromusculoskeletal simulation could help to target appropriate therapies. Furthermore, therapies such as drugs or epidural electrical stimulation themselves could be simulated to study their efficiency.

References

Af Klint, R., Mazzaro, N., Nielsen, J., Sinkjaer, T., & Grey, M. (2010). Load rather than length sensitive feedback contributes to soleus muscle activity during human treadmill walking. *Journal of Neurophysiology*, **103**(5), 2747–2756.

Alvarez, C., De Vera, M., Beauchamp, R., Ward, V., & Black, A. (2007). Classification of idiopathic toe walking based on gait analysis: Development and application of the ITW severity classification. *Gait & Posture*, **26**(3), 428–435.

Aoi, S., Ohashi, T., Bamba, R., Fujiki, S., Tamura, D., & Funato, T. (2019). Neuromusculoskeletal model that walks and runs across a speed range with a few motor control parameter changes based on the muscle synergy hypothesis. *Scientific Reports*, **9**(1), 1–13.

Armand, S., Decoulon, G., & Bonnefoy-Mazure, A. (2016). Gait analysis in children with cerebral palsy. *EFORT Open Reviews*, **1**(12), 448–460.

Attias, M., Bonnefoy-Mazure, A., De Coulon, G., Cheze, L., & Armand, S. (2017). Influence of different degrees of bilateral emulated contractures at the triceps surae on gait kinematics. *Gait & Posture*, **58**, 176–182.

Bohannon, R. (2007). Muscle strength and muscle training after stroke. *Journal of Rehabilitation Medicine*, **39**(1), 14–20.

Boschges, A., & El Manira, A. (1998). Sensory pathways and their modulation in the control of locomotion. *Current Opinion in Neurobiology*, **8**(6), 733–739.

Brockett, C., & Chapman, G. (2016). Biomechanics of the ankle. *Orthopaedics and Trauma*, **30**(3), 232–238.

Calancie, B., Broton, J., Klose, K., Traad, M., Difini, J., & Ayyar, D. (1993). Evidence that alterations in presynaptic inhibition contribute to segmental hypo- and hyper-excitability after spinal cord injury in man. *Electroencephalography and Clinical Neurophysiology*, **89**(3), 177–186.

Chia, K., Fischer, I., Thomason, P., Graham, H., & Sangeux, M. (2020). A decision support system to facilitate identification of musculoskeletal impairments and propose recommendations using gait analysis in children with cerebral palsy. *Frontiers in Bioengineering and Biotechnology*, **8**, 529415.

Crenna, P. (1998). Spasticity and 'spastic' gait in children with cerebral palsy. *Neuroscience & Biobehavioral Reviews*, **22**, 571–578.

Crone, C., Hultborn, H., Jespersen, B., & Nielsen, J. (1987). Reciprocal ia inhibition between ankle flexors and extensors in man. *Journal of Physiology*, **389**(1), 163–185.

Crone, C., Johnsen, L., Biering-Sørensen, F., & Nielsen, J. (2003). Appearance of reciprocal facilitation of ankle extensors from ankle flexors in patients with stroke or spinal cord injury. *Brain*, **126**(2), 495–507.

Delp, S., Loan, J., Hoy, M., Zajac, F., Topp, E., & Rosen, J. (1990). An interactive graphics-based model of the lower extremity to study orthopaedic surgical procedures. *IEEE Transactions on Biomedical Engineering*, **37**(8), 757–767.

Di Russo, A., Stanev, D., Armand, S., & Ijspeert, A. (2021). Sensory modulation of gait characteristics in human locomotion: A neuromusculoskeletal modeling study. *PLOS Computational Biology*, **17**(5), e1008594.

Dietz, V., & Sinkjaer, T. (2007). Spastic movement disorder: Impaired reflex function and altered muscle mechanics. *Lancet Neurology*, **6**(8), 725–733.

Diong, J., Herbert, R. D., Harvey, L. A., Kwah, L. K., Clarke, J. L., Hoang, P. D., Martin, J. H., Clarke, E. C., Bilston, L. E., & Gandevia, S. C. (2012). Passive mechanical properties of the gastrocnemius after spinal cord injury. *Muscle & Nerve*, **46**(2), 237–245.

Elder, G. C., Kirk, J., Stewart, G., Cook, K., Weir, D., Marshall, A., & Leahey, L. (2003). Contributing factors to muscle weakness in children with cerebral palsy. *Developmental Medicine and Child Neurology*, **45**(8), 542–550.

Faist, M., Dietz, V., & Pierrot-Deseilligny, E. (1995). Modulation, probably presynaptic in origin, of mono-synaptic ia excitation during human gait. *Experimental Brain Research*, **109**, 441–449.

Faist, M., Hoefer, C., Hodapp, M., Dietz, V., Berger, W., & Duysens, J. (2006). In humans b facilitation depends on locomotion while suppression of ib inhibition requires loading. *Brain Research*, **1076**(1), 87–92.

Faist, M., Mazevet, D., Dietz, V., & Pierrot-Deseilligny, E. (1994). A quantitative assessment of presynaptic inhibition of ia afferents in spastics. *Brain*, **117**(6), 1449–1455.

Falisse, A., Bar-On, L., Desloovere, K., Jonkers, I., & De Groote, F. (2018). A spasticity model based on feedback from muscle force explains muscle activity during passive stretches and gait in children with cerebral palsy. *Plos One*, **13**(12), e0208811.

Frijns, C., Laman, D., Van Duijn, M., & Van Duijn, H. (1997). Normal values of patellar and ankle tendon reflex latencies. *Clinical neurology and Neurosurgery*, **99**(1), 31–36.

Geijtenbeek, T. (2019). Scone: Open source software for predictive simulation of biological motion. *Journal of Open Source Software*, **4**(38), 1421.

Geyer, H., & Herr, H. (2010). A muscle-reflex model that encodes principles of legged mechanics produces human walking dynamics and muscle activities. *IEEE Transactions on Neural Systems and Rehabilitation Engineering*, **18**(3), 263–273.

Granata, K. P., Abel, M. F., & Damanio, D. L. (2000). Joint angular velocity in spastic gait and the influence of muscle–tendon lengthening. *Journal of Bone and Joint Surgery*, **82**(2), 174–186.

Hunt, K., & Crossley, F. (1975). Coefficient of restitution interpreted as damping in vibroimpact. *Journal of Applied Mechanics*, **42**(2), 440–445.

Igel, C., Hansen, N., & Roth, S. (2007). Covariance matrix adaptation for multi-objective optimization. *Evolutionary Computation*, **15**(1), 1–28.

James, G., Schwartz, M., Koop, S., & TF, N. (2009). *The identification and treatment of gait problems in cerebral palsy*. John Wiley & Sons.

Jansen, K., De Groote, F., Aerts, W., De Schutter, J., Duysens, J., & Jonkers, I. (2014). Altering length and velocity feedback during a neuro-musculoskeletal simulation of normal gait contributes to hemiparetic gait characteristics. *Journal of NeuroEngineering and Rehabilitation*, **11**(1), 78.

Kerkum, Y. L., Buizer, A. I., van den Noort, J. C., Becher, J. G., Harlaar, J., & Brehm, M. A. (2015). The effects of varying ankle foot orthosis stiffness on gait in children with spastic cerebral palsy who walk with excessive knee flexion. *Plos One*, **10**(11), e0142878.

Kiehn, O. (2016). Decoding the organization of spinal circuits that control locomotion. *Nature Reviews Neuroscience*, **17**(4), 224–238.

Knikou, M. (2010). Neural control of locomotion and training-induced plasticity after spinal and cerebral lesions. *Clinical Neurophysiology*, **121**(10), 1655–1668.

Knikou, M., & Mummidisetty, C. (2011). Reduced reciprocal inhibition during assisted stepping in human spinal cord injury. *Experimental Neurophysiology*, **231**:104–112.

Kuo, A., & Ryu, H. (2021). An optimality principle for locomotor central pattern generators. *Scientific Reports*, **11**(1), 13140.

Lamontagne, A., Malouin, F., Richards, C., & Dumas, F. (2002). Mechanisms of disturbed motor control in ankle weakness during gait after stroke. *Gait & Posture*, **15**, 244–255.

Lance, J., Feldman, R., Young, R., & Koella, W. (1980). Pathophysiology of spasticity and clinical experience with baclophen. *Spasticity: Disordered Motor Control*, 485–495.

Leech, K., Kim, H., & Horny, T. (2018). Strategies to augment volitional and reflex function may improve locomotor capacity following incomplete spinal cord injury. *Journal of Neurophysiology*, **119**(3), 894–903.

Levin, M. F., & Feldman, G. (1994). The role of stretch reflex threshold regulation in normal and impaired motor control. *Brain Research*, **657**(1–2), 23–30.

Lenhart, R. L., Francis, C. A., Lenz, A. L., & Thelen, D. G. (2014). Empirical evaluation of gastrocnemius and soleus function during walking. *Journal of Biomechanics*, **47**(12), 2969–2974.

Lieber, R., Steinman, S., Barashi, I., & Chambers, H. (2004). Structural and functional changes in spastic skeletal muscle. *Muscle & Nerve*, **29**(5), 615–627.

Lorentzena, J., Greyb, M. J., Crone, C., Mazevete, D., Biering-Sørensend, F., & Nielsenb, J. B. (2010). Distinguishing active from passive components of ankle plantar flexor stiffness in stroke, spinal cord injury and multiple sclerosis. *Clinical Neurophysiology*, **121**(11), 1939–1951.

Lundberg, A., Malmgren, K., & Schomburg, E. (1987). Reflex pathways from group ii muscle afferents. *Experimental Brain Research*, **65**(2), 294–306.

Marque, P., Simonetta-Moreau, M., Maupas, E., & CF, R. (2001). Facilitation of transmission in heteronymous group ii pathways in spastic hemiplegic patients. *Journal of Neurology, Neurosurgery and Psychiatry*, **70**(1), 36–42.

Matjacic, Z., Olensek, A., & Bajd, T. (2006). Biomechanical characterization and clinical implications of artificially induced toe-walking: Differences between pure soleus, pure gastrocnemius and combination of soleus and gastrocnemius contractures. *Journal of Biomechanics*, **39**(2), 255–266.

Meunier, S., & Pierrot-Deseilligny, E. (1998). Cortical control of presynaptic inhibition of ia afferents in humans. *Experimental Brain Research*, **119**(4), 415–426.

Millard, M., Uchida, T., Seth, A., & Delp, S. (2013). Flexing computational muscle: Modeling and simulation of musculotendon dynamics. *Journal of Biomechanical Engineering*, **135**(2), 0210051–02100511.

Minassian, K., Hofstoetter, U., Dzeladini, F., Guertin, P., & Ijspeert, A. (2017). The human central pattern generator for locomotion: Does it exist and contribute to walking? *The Neuroscientist*, **23**(6), 649–663.

Mirbagheri, M. M., Barbeau, H., Ladouceur, M., & Kearney, R. E. (2001). Intrinsic and reflex stiffness in normal and spastic, spinal cord injured subjects. *Experimental Brain Research*, **141**, 446–459.

Neyroud, D., Armand, S., De Coulon, G., Da Silva, S. R. D., Maffiuletti, N. A., Kayser, B., & Place, N. (2017). Plantar flexor muscle weakness and fatigue in spastic cerebral palsy patients. *Research in Developmental Disabilities*, **61**, 66–76.

Nieuwenhuys, A., Ounpuu, S., Van Campenhout, A., Theolohis, T., De Cat, J., Stout, J., Molenaers, G., De Laet, T., & Desloovere, K. (2015). Identification of joint patterns during gait in children with cerebral palsy: A delphi consensus study. *Developmental Medicine & Child Neurology*, **58**(3), 306–313.

Ong, C., Geijtenbeek, T., Hicks, J., & Delp, S. (2019). Predicting gait adaptations due to ankle plantar flexor muscle weakness and contracture using physics-based musculoskeletal simulations. *PLOS Computational Biology*, **15**(10), e1006993.

Papadonikolakis, A., Vekris, M., Korompilias, A., Kostas, J., Ristanis, S., & Soucacos, P. (2003). Botulinum a toxin for treatment of lower limb spasticity in cerebral palsy gait analysis in 49 patients. *Acta Orthopaedica*, **74**(6), 749–755.

Perry, J., & Burnfield, J. (2010a). *Gait analysis: Normal and pathological function*. SLACK Inc.

Perry, J., & Burnfield, J. (2010b). *Gait analysis: normal and pathological function*, vol. **1**(12). Slack Incorporated.

Petersen, N., Morita, H., & Nielsen, J. (1999). Modulation of reciprocal inhibition between ankle extensors and flexors during walking in man. *Journal of Physiology*, **520**(2), 605.

Pierrot-Deseilligny, E., & Burke, D. (2012). *The circuitry of the human spinal cord: spinal and corticospinal mechanisms of movement*. Cambridge University Press.

Prochazka, A. (1989). Sensorimotor gain control: A basic strategy of motor systems? *Progress in Neurophysiology*, **33**(4), 281–307.

Prochazka, A. (1999). Chapter 11 quantifying proprioception. *Progress in Brain Research*, **123**, 133–142.

Rossignol, S., Dubuc, R., & Gossard, J. (2006). Dynamic sensorimotor interactions in locomotion. *Physiological Reviews*, **86**(1), 89–154.

Schwartz, M., Rozumalski, A., & Trost, J. (2008). The effect of walking speed on the gait of typically developing children. *Journal of Biomechanics*, **41**(8), 1639–1650.

Sinkjær, T., Andersen, J., Ladouceur, M., Christensen, L., & Nielsen, J. (2000). Major role for sensory feedback in soleus emg activity in the stance phase of walking in man. *Journal of Physiology*, **523**(3), 817–827.

Smith, A. C., Rymer, W. Z., & Knikou, M. (2015). Locomotor training modifies soleus monosynaptic motoneuron responses in human spinal cord injury. *Experimental Brain Research*, **233**(1), 89-103.

Song, S., & Geyer, H. (2015). A neural circuitry that emphasizes spinal feedback generates diverse behaviours of human locomotion. *The Journal of Physiology*, **593**(16), 3493–3511.

Song, S., & Geyer, H. (2018). Predictive neuromechanical simulations indicate why walking performance declines with ageing. *The Journal of Physiology*, **596**(7), 1199–1210.

Steele, K., van der Krogt, M. M., Schwartz, M., & Delp, S. (2012). How much muscle strength is required to walk in a crouch gait? *Journal of Biomechanics*, **45**(15), 2564–2569.

Stephens, M., & Yang, J. (1996). Short latency, non-reciprocal group i inhibition is reduced during the stance phase of walking in humans. *Experimental Brain Research*, **743**(1–2), 24–31.

Taga, G. (1995). A model of the neuro-musculoskeletal system for human locomotion. *Biological Cybernetics*, **73**(2), 97–111.

Thomas, C., Zaidner, E., Calancie, B., Broton, J., & Bigland-Ritchie, B. (1997). Muscle weakness, paralysis, and atrophy after human cervical spinal cord injury. *Experimental Neurology*, **148**(2), 414–423.

Thomas, C. K., Bakels, R., Klein, C. S., & Zijdewind, I. (2014). Human spinal cord injury: Motor unit properties and behaviour. *Acta Physiologica*, **210**(1), 5–19.

Van der Krogt, M. M., Doorenbosch, C. A., Becher, J. G. S. J. S., & Harlaar, J. (2010). Dynamic spasticity of plantar flexor muscles in cerebral palsy gait. *Journal of Rehabilitation Medicine*, **42**(7), 656–663

Van der Krogt, M. M., Bar-On, L., Kindt, T., Desloovere, K., & Harlaar, J. (2016). Neuromusculoskeletal simulation of instrumented contracture and spasticity assessment in children with cerebral palsy. *Journal of NeuroEngineering Rehabilitation*, **13**(1), 64.

Van Der Salm, A., Nene, A., DJ, M., Veltink, P., Hermens, H., & IJzerman, M. (2005). Gait impairments in a group of patients with incomplete spinal cord injury and their relevance regarding therapeutic approaches using functional electrical stimulation. *Artificial Organs*, **29**(1), 8–14.

Veerkamp, K., Waterval, N., Geijtenbeek, T., Carty, C., Lloyd, D., Harlaar, J., & van der Krogt, M. M. (2021). Evaluating cost function criteria in predicting healthy gait. *Journal of Biomechanics*, **123**, 110530.

Wang, J., Hamner, S., Delp, S., & Koltun, V. (2012). Optimizing locomotion controllers using biologically-based actuators and objectives. *ACM Transactions on Graphics*, **31**(4), 1.

Waterval, N., Veerkamp, K., Geijtenbeek, T., Harlaar, J., Nollet, F., Brehm, M., & van der Krogt, M. M. (2021). Validation of forward simulations to predict the effects of bilateral plantar flexor weakness on gait. *Gait & Posture*, **87**, 33–42.

Xia, R., & Rymer, W. (2005). Reflex reciprocal facilitation of antagonist muscles in spinal cord injury. *Spinal Cord*, **43**(1), 14–21.

Yang, J., Stein, R., & James, K. (1991). Contribution of peripheral afferents to the activation of the soleus muscle during walking in humans. *Experimental Brain Research*, **87**(3), 679–687.

Zehr, E., & Stein, R. (1999). What functions do reflexes serve during human locomotion? *Progress in Neurobiology*, **58**(2), 185–205

Additional information

Data availability statement

All the necessary files to reproduce this study are provided in the following GitHub repository, whose structure is detailed in its ReadMe file: https://github.com/AliceBrue/pathological_gait.git

We also used healthy gait data from Schwartz et al. (2008) and Perry and Burnfield (2010a) as references in our plots.

Competing interests

None of the authors has any conflicts of interests.

Authors contribution

A.B. contributed to the design of the work, to the generation, analysis and interpretation of the simulations, and to the writing of the manuscript. S.B.G. contributed to the generation and analysis of the simulations. A.D.R. contributed to the conception and design of the work, and to the revision of the manuscript. D.S. contributed to the conception and design of the work, and to the revision of the manuscript. S.A. contributed to the interpretation of the simulations, and to the revision of the manuscript. G.C. contributed to the revision of the manuscript. A.I. contributed to the conception of the work and to the revision of the manuscript.

All authors approved the final version of the manuscript. All authors agree to be accountable for all aspects of the work in ensuring that questions related to the accuracy or integrity of any part of the work are appropriately investigated and resolved. All persons designated as authors qualify for authorship, and all those who qualify for authorship are listed.

Supporting information

Additional supporting information can be found online in the Supporting Information section at the end of the HTML view of the article. Supporting information files available:

Statistical Summary Document
Peer Review History